Inorganic Chemistry

Article

pubs.acs.org/IC

Mn^{2+} Complexes with 12-Membered Pyridine Based Macrocycles Bearing Carboxylate or Phosphonate Pendant Arm: Crystallographic, Thermodynamic, Kinetic, Redox, and $^{1}H/^{17}O$ Relaxation Studies

Bohuslav Drahoš,[†,‡] Jan Kotek,[†] Ivana Císařová,[†] Petr Hermann,[†] Lothar Helm,[§] Ivan Lukeš,*[,†] and Éva Tóth*[,‡]

[†]Department of Inorganic Chemistry, Faculty of Science, Universita Karlova (Charles University), Hlavova 2030, 128 43 Prague 2, Czech Republic

[‡]Centre de Biophysique Moléculaire, CNRS, rue Charles Sadron, 45071 Orléans, France

[§]Ecole Polytechnique Fédérale de Lausanne, BCH, Lausanne, Switzerland

Supporting Information

ABSTRACT: Mn^{2+} complexes represent an alternative to Gd^{3+} chelates which are widely used contrast agents in magnetic resonance imaging. In this perspective, we investigated the Mn^{2+} complexes of two 12-membered, pyridine-containing macrocyclic ligands bearing one pendant arm with a carboxylic acid (HL^1, 6-carboxymethyl-3,6,9,15-tetraazabicyclo[9.3.1] pentadeca-1(15),11,13-triene) or a phosphonic acid function (H_2L^2, 6-dihydroxyphosphorylmethyl-3,6,9,15-tetraazabicyclo[9.3.1]pentadeca-1(15),11,13-triene). Both ligands were synthesized using nosyl or tosyl amino-protecting groups (starting from diethylenetriamine or tosylaziridine). The X-ray crystal structures confirmed a coordination number of 6 for Mn^{2+} in their complexes. In aqueous solution, these pentadentate ligands allow one free coordination site for a water molecule. Potentiometric titration data indicated a higher basicity for H_2L^2 than that for HL^1, related to the electron-donating effect of the negatively charged phosphonate group. According to the protonation sequence determined by ^{1}H and ^{31}P pH-NMR titrations, the first two protons are attached to macrocyclic amino groups whereas the subsequent protonation steps occur on the pendant arm. Both ligands form thermodynamically stable complexes with Mn^{2+}, with full complexation at physiological pH and 1:1 metal to ligand ratio. The kinetic inertness was studied via reaction with excess of Zn^{2+} under various pHs. The dissociation of MnL^2 is instantaneous (at pH 6). For MnL^1, the dissociation is very fast ($k_{obs} = 1-12 \times 10^3$ s^{-1}), much faster than that for MnDOTA, MnNOTA, or the Mn^{2+} complex of the 15-membered analogue. It proceeds exclusively via the dissociation of the monoprotonated complex, without any influence of Zn^{2+}. In aqueous solution, both complexes are air-sensitive leading to Mn^{3+} species, as evidenced by UV−vis and ^{1}H NMRD measurements and X-ray crystallography. Cyclic voltammetry gave low oxidation peak potentials ($E_{ox} = 0.73$ V for MnL^1 and $E_{ox} = 0.68$ V for MnL^2), in accordance with air-oxidation. The parameters governing the relaxivity of the Mn^{2+} complexes were determined from variable-temperature ^{17}O NMR and ^{1}H NMRD data. The water exchange is extremely fast, $k_{ex} = 3.03$ and 1.77×10^9 s^{-1} for MnL^1 and MnL^2, respectively. Variable-pressure ^{17}O NMR measurements have been performed to assess the water exchange mechanism on MnL^1 and MnL^2 as well as on other Mn^{2+} complexes. The negative activation volumes for both MnL^1 and MnL^2 complexes confirmed an associative mechanism of the water exchange as expected for a hexacoordinated Mn^{2+} ion. The hydration number of $q = 1$ was confirmed for both complexes by ^{17}O chemical shifts. A relaxometric titration with phosphate, carbonate or citrate excluded the replacement of the coordinated water molecule by these small endogenous anions.

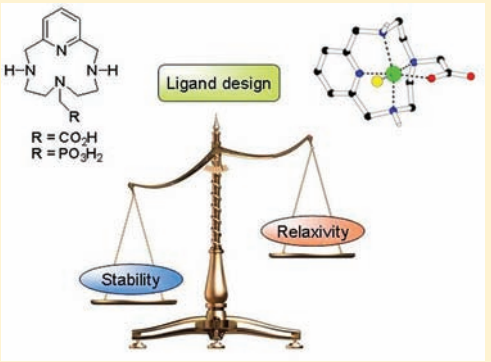

INTRODUCTION

Recently, considerable attention has been focused on manganese(II) complexes as an alternative to Gd^{3+} chelates for Contrast Agent (CAs) applications in Magnetic Resonance Imaging (MRI).[1−3] Today, paramagnetic Gd^{3+} complexes represent the majority of clinical CAs. They enhance the longitudinal ($1/T_1$) relaxation of water protons in body tissues resulting in a positive contrast in T_1-weighted MR images. The CA efficiency is described by the proton relaxivity (r_1) which is defined as the paramagnetic enhancement of the longitudinal relaxation rate of water protons in 1 mM solution of the CA. Relaxivity has inner- and outer-sphere contributions.[4] The inner-sphere relaxivity[4] is mainly governed by the number of coordinated water molecules (hydration number q), the water exchange rate (k_{ex}, residence time τ_M; $\tau_M = 1/k_{ex}$), the rotational correlation time (τ_R), and electron spin relaxation (T_{ie}, i = 1,2); some of these parameters can be tuned by appropriate ligand design to optimize relaxivity.[5,6]

Given its five unpaired electrons and slow electronic relaxation, manganese(II) is an interesting metal ion for MRI applications.

Received: September 2, 2011
Published: November 17, 2011

Chart 1. Structures of the Ligands Studied and Discussed in the Text[a]

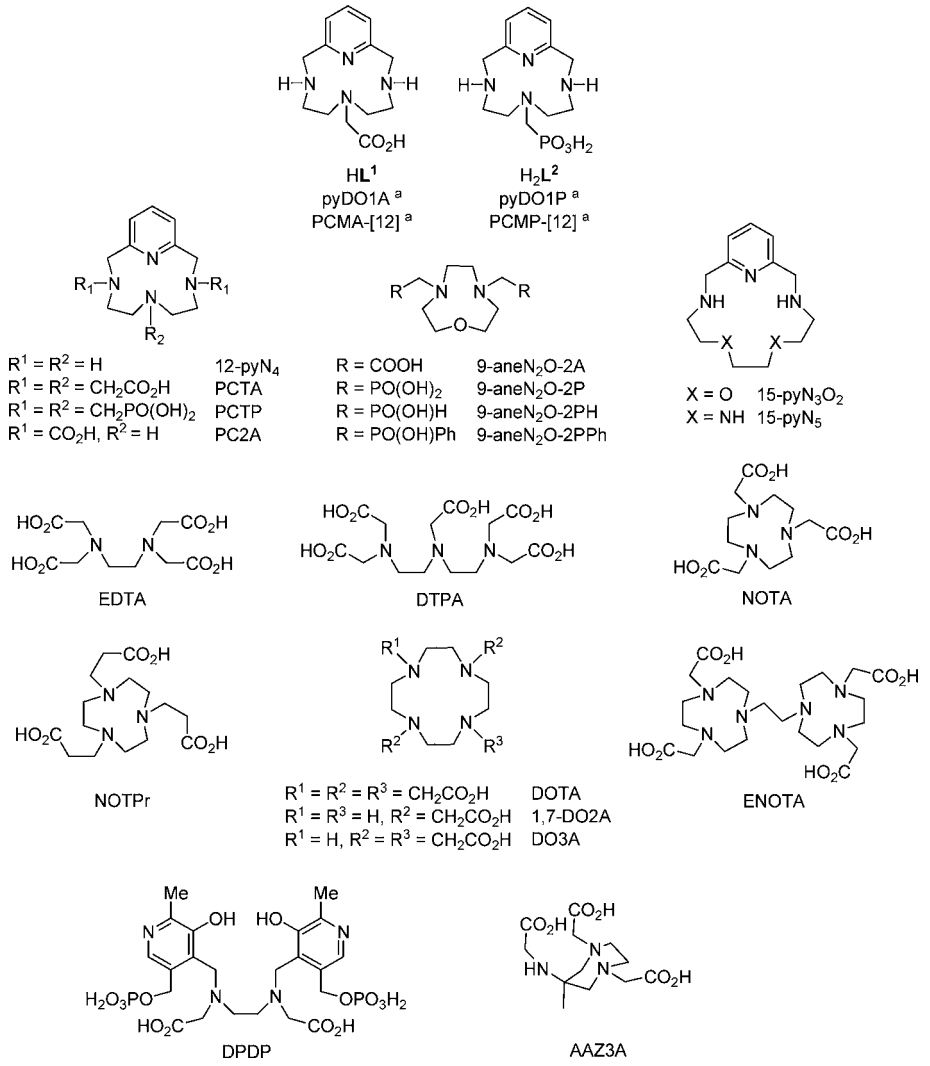

[a]The superscript "a" indicates abbreviations frequently used in previous papers.

The water exchange rate on Mn^{2+} complexes is usually fast and can allow for attaining high relaxivities, while it can be a limiting factor for Gd^{3+} chelates. Manganese has an important role in biological systems.[7,8] Because of its similar ionic radius to Ca^{2+}, Mn^{2+} is a Ca^{2+} competitor in many biological processes which allows the detection of calcium influx and calcium distribution in the central nervous system.[9] Manganese Enhanced MRI (MEMRI)[10] applies free Mn^{2+} for detailed monitoring of brain or heart structure and provides insight into neuroanatomy, neuroconnectivity, neuronal function, and neuropathology.[11] However, the toxicity of the manganese salts at concentrations providing sufficient contrast limits this method to animal studies.[12] Higher concentrations of free Mn^{2+} lead to a form of parkinsonism (manganism)[12] primarily caused by damage of the basal ganglia. This observation was supported by accumulation of Mn^{2+} in the brain.[13]

High thermodynamic stability and kinetic inertness are the prerequisite for safe in vivo use of Mn^{2+} complex as a CA. The lack of ligand-field stabilization energy caused by the high-spin d^5 electron configuration and the smaller charge of Mn^{2+} induce lower thermodynamic stability as compared to other transition metal ions or Gd^{3+} complexes. Although Mn^{2+} complexes were considered as kinetically labile,[13] recent dissociation kinetic data have evidenced that Mn^{2+} chelates of NOTA and DOTA, both nonhydrated, have remarkable kinetic inertness.[14] However, in general it is difficult to consolidate sufficient thermodynamic stability and kinetic inertness with the efforts to increase the number of inner-sphere water molecules.

There is only one Mn^{2+} complex clinically approved ($[Mn(dpdp)]^{4-}$, Teslascan, $dpdp^{6-}$ = *N*,*N*′-dipyridoxylethylenediamine-*N*,*N*′-diacetate-5,5′-bis(phosphate))[15] for liver, kidney, and cardiac imaging. The complex itself contains no inner-sphere water molecule, and the observed in vivo relaxation enhancement arises from the release of free Mn^{2+} in the body. Mn^{2+} complexes of the linear polydentate ligands EDTA[16−19] or DTPA[20] and macrocyclic derivatives of NOTA,[21,22] DOTA,[18,21,23,24] or AAZ3A[25] have been investigated with respect to their relaxation efficacy (Chart 1). These ligands, originally mostly designed for Gd^{3+}, allow for maximum one inner-sphere water molecule in the Mn^{2+} complex except the 15-membered azacrown-ethers[26] that form bishydrated Mn^{2+} complexes.

The preferred coordination number of Mn^{2+} is 6 or 7 and therefore the maximum number of donor atoms in the ligand must not exceed 6 as at least one coordination site has to be accessible for water binding. Some hexadentate ligands do not ensure either a coordinated water molecule. With this in mind,

dx.doi.org/10.1021/ic201935r | Inorg. Chem. 2011, 50, 12785–12801

Table 1. Crystallographic Parameters of the Studied Compound

	$(H_3\text{-}12\text{-}pyN_4)Br_3$	$(H_4L^2)(H_3L^2)Br_3\cdot 0.5H_2O$	$[Mn(L^1)Cl]\cdot 1.5H_2O$	$[Mn(L^2)]\cdot 1/6NaCl\cdot 1/3LiOH\cdot 9H_2O$	$[Mn(L^2)(OH)]\cdot 0.5LiCl\cdot 7H_2O$
M_r	449.05	851.35	380.74	922.05	517.54
color, habit	colorless plate	colorless plate	light pink plate	yellow plate	dark red rod
crystal system	monoclinic	triclinic	triclinic	hexagonal	monoclinic
space group	$P2_1/c$	$P\bar{1}$	$P\bar{1}$	$P\bar{3}$	$C2/c$
a (Å)	7.57620(10)	7.8242(2)	8.5501(3)	19.5953(3)	27.5708(4)
b (Å)	13.5659(3)	14.8593(3)	8.8443(2)	19.5953(3)	8.8310(2)
c (Å)	15.3629(3)	16.3673(4)	11.3487(3)	19.3343(3)	20.1313(4)
α (deg)	90.00	66.0230(11)	98.7253(16)	90.00	90.00
β (deg)	97.7961(12)	77.9301(12)	100.1819(14)	90.00	114.7855(10)
γ (deg)	90.00	87.3948(13)	102.9234(15)	120.00	90.00
U, Å^3	1564.37(5)	1698.59(7)	806.75(4)	6429.28(17)	4450.01(15)
Z	4	2	2	6	8
D_{calc}, g cm^{-3}	1.907	1.665	1.567	1.429	1.545
μ, mm^{-1}	7.727	3.708	1.005	0.759	0.785
total refl.	3589	7786	3696	8434	5117
obsd. refl. ($I > 2\sigma(I)$)	2992	6097	3226	6909	4219
R, $R'(I > 2\sigma(I))$	0.0362, 0.0258	0.0482, 0.0303	0.0366, 0.0307	0.0724, 0.0565	0.0444, 0.0339
wR, $wR'(I > 2\sigma(I))$	0.0596, 0.0565	0.0724, 0.0672	0.0835, 0.0808	0.1668, 0.1565	0.0932, 0.0883

we have designed a series of pentadentate ligands. The 15-membered pyridine based macrocycles[27] have been studied which have two inner-sphere water molecules in their Mn^{2+} complexes (CN = 7, CN = Coordination Number). Recently, Mn^{2+} complexes of 9-membered ligands based on 1-oxa-4,7-diazacyclononane derivatives with different pendant arms have been reported[28] (one inner-sphere water molecule, CN = 6). These studies allowed us to conclude that Mn^{2+} prefers macrocycles containing rather nitrogen than oxygen donor atoms and that the complex stability increases with the size of the macrocyclic cavity (9→15-membered) and with increasing ligand basicity. In addition, the presence of the pyridine rigidifies the macrocyclic cavity and, therefore, increases the complex stability. A phosphonate functional group in the pendant arm appeared to improve the complex stability (higher ligand basicity) as well as the relaxivity. On the basis of these observations, we have developed pentadentate, 12-membered, pyridine-containing macrocyclic ligands that bear one pendant arm with a carboxylic (HL^1) or phosphonic (H_2L^2) acid group (Chart 1).

Here we report the synthesis of ligands HL^1 and H_2L^2. The structure of the protonated ligands and their Mn^{2+} complexes was confirmed by X-ray analysis, and the Mn^{3+} complex of H_2L^2 is also described. The protonation constants of the ligands and the stability constants of their complexes with Mn^{2+} and other selected metal ions were determined by potentiometry. The kinetic inertness of their Mn^{2+} complexes was investigated by reaction with Zn^{2+} at various pHs using relaxometry. Variable-temperature ^{17}O NMR and ^1H NMRD measurements allowed calculation of the microscopic parameters governing the relaxivity. Variable-pressure ^{17}O relaxation rates were measured to assess the mechanism of water exchange. The air oxidation of both Mn^{2+} complexes was confirmed by UV−vis spectra and cyclic voltammetry. These results are discussed in comparison to the data for the 9- and 15-membered analogues that we have previously reported.

EXPERIMENTAL SECTION

Solvents were dried by standard procedures,[29] distilled under argon and stored over 4 Å molecular sieves in argon atmosphere: Toluene (Penta, distilled from K), MeCN (Penta, distilled from P_2O_5), tetrahydrofuran (THF; Penta, distilled from Na/K), dimethylformamide (DMF; Penta, distilled from BaO). Diethyl aminomethylphosphonate,[30] *N*-(4-methylbenzenesulfonyl)aziridine,[31] ditosylated amine **1a**, 4-[(diethoxyphosphoryl)-methyl]-1,7-bis(4-methylbenzenesulfonyl)-1,4,7-triazaheptane,[32] 1,7-bis(2-nitrobenzenesulfonyl)-1,4,7-triazaheptane,[33] 4-[(*t*-butoxycarbonyl)methyl]-1,7-bis(2-nitrobenzenesulfonyl)-1,4,7-triazaheptane,[33] protected cycle **2a**, 6-[(diethoxyphosphoryl)methyl]-3,9-bis(4-methylbenzenesulfonyl)-3,6,9,15-tetraazabicyclo[9.3.1]pentadeca-1(15),11,13-triene,[32] and **2b**, 6-[(*t*-butoxycarbonyl)methyl]-3,9-bis(2-nitrobenzenesulfonyl)-3,6,9,15-tetraazabicyclo[9.3.1]pentadecane-1(15),11,13-triene,[33] using a precursor 2,6-bis(bromomethyl)pyridine[34,35] were synthesized by literature procedures. The 1,4,7-triazaheptane and other chemicals and solvents were purchased from commercial sources and used as received.

NMR spectra were recorded at 25 °C on a Varian VNMRS300 spectrometer: ^1H 299.9 MHz, TMS (internal) δ = 0.0 ppm; ^{13}C 75.4 MHz, TMS (internal) δ = 0.0 ppm; $CHCl_3$ (internal) δ = 77.0 ppm; ^{31}P 121.4 MHz, 85% aq. H_3PO_4 (external) δ = 0.0 ppm or a Bruker Avance 500 MHz spectrometer: ^1H 500.1 MHz; ^{13}C 125.8 MHz; ^{31}P 202.5 MHz with the same internal or external references. Multiplicity of the signals is indicated as follows: s, singlet; d, doublet; t, triplet; q, quartet; m, multiplet; br, broad. Deuterated solvent $CDCl_3$ and D_2O (99.8% D) from Chemotrade was used as received. Mass spectra were measured on a Bruker spectrometer ESQUIRE 3000 equipped with an electro-spray ion source and ion-trap detector in positive/negative mode and on an Autoflex instrument (Bruker Daltonics, Bremen, Germany) using MALDI-TOF ionization/detection technique. For thin layer chromatography, Merck aluminum foils with silica gel 60 F254 impregnated with a fluorescent dye were used. Elemental analyses were done at the Institute of Macromolecular Chemistry (Academy of Science of the Czech Republic, Prague).

Crystal Structure Determination. Selected crystals were mounted on a glass fiber in random orientation and cooled to 150(1) K. The diffraction data were collected employing a Nonius Kappa CCD diffractometer (Enraf-Nonius) using Mo-K_α (λ = 0.71073 Å) at 150(1) K (Cryostream Cooler Oxford Cryosystem) and analyzed using the HKL DENZO program package.[36] The structures were solved by direct methods and refined by full-matrix least-squares techniques [SIR92 (ref 37) and SHELXL97 (ref 38)], and the experimental crystallographic data are listed in Table 1.

The used scattering factors for neutral atoms were included in the SHELXL97 program. The crystals of $(H_3\text{-}12\text{-}pyN_4)Br_3$ were prepared by slow concentration of a 12-pyN_4 solution in diluted HBr. The independent unit contains one triprotonated macrocyclic molecule and three isolated bromide anions. All non-hydrogen atoms were refined anisotropically. All hydrogen atoms were found in the electron density

dx.doi.org/10.1021/ic201935r | *Inorg. Chem.* 2011, 50, 12785–12801

difference map; however, in the final refinement cycles, they were fixed in theoretical (C−H) or in original (N−H) positions.

The crystals of $(H_4L^2)(H_3L^2)Br_3{\cdot}0.5H_2O$ were prepared by slow vapor diffusion of acetone into H_2L^2 solution in diluted aqueous HBr. The independent unit contains two differently protonated ligand molecules, the first 4-fold and the second 3-fold, and the charge is compensated by three bromide anions. The water solvate molecule was best refined as half-occupied to keep thermal factors reasonable. All non-hydrogen atoms were refined anisotropically. All hydrogen atoms were found in the electron density difference map, and were fixed in theoretical (C−H) or in original (N−H, O−H) positions.

The $[Mn(\mathbf{L^1})Cl]{\cdot}1.5H_2O$ crystals suitable for X-ray analysis were prepared by vapor diffusion of acetone into the deoxygenated aqueous solution of the Mn^{2+} complex prepared from solid $MnCl_2{\cdot}4H_2O$ and $H\mathbf{L^1}$ using 10% ligand excess; the pH was adjusted by aq. NaOH to ∼8. One of the water solvate molecules was best refined as half-occupied to keep thermal factors reasonable. All non-hydrogen atoms were refined anisotropically. All hydrogen atoms were found in the electron density difference map, and were fixed in theoretical (C−H) or in original (N−H, O−H) positions.

From a deoxygenated methanolic mixture of $Mn(ClO_4)_2{\cdot}4H_2O$−$H_2\mathbf{L^2}$−LiOH (10% ligand excess, formal pH adjusted to ∼8 according to pH-strip) prepared under inert argon atmosphere, single-crystals suitable for X-ray diffraction study were formed after acetone vapor diffusion into the solution at 5 °C. To avoid the presence of chloride ions, the original ligand hydrochloride was purified on a cation exchange column. The X-ray analysis revealed a composition which was best formulated as $[Mn(\mathbf{L^2})]{\cdot}1/6NaCl{\cdot}1/3LiOH{\cdot}9H_2O$. This composition seems rather improbable, and given the problems with the interpretation of the electronic maxima because of rather bad diffraction data, we isolated a new batch of crystals from a newly prepared solution. However, the diffraction pattern of the new crystals was the same, and the structure refinement revealed electronic maxima in identical positions as in the first case. Although one can have doubts associated with the assignment of the chloride counterion and the disordered water molecules, the structure of the complex molecules is unambiguous. All non-hydrogen atoms were refined anisotropically. Almost all hydrogen atoms were found in the electron density difference map, and were fixed in theoretical (C−H) or in original (N−H, O−H) positions. For electroneutrality reasons, one of the diffraction maxima attributed to oxygen atoms is probably a hydroxide anion instead of a water molecule.

Suitable crystals of $[Mn(\mathbf{L^2})(OH)]{\cdot}0.5LiCl{\cdot}7H_2O$ were prepared by acetone vapor diffusion into a MeOH solution of a $MnCl_2{\cdot}4H_2O$−$H_2\mathbf{L^2}$ mixture under air atmosphere (10% ligand excess) with a formal pH adjusted to ∼8 (pH-strip) by LiOH. The independent unit is formed by a complex molecule, a Li^+ aqua ion, an isolated chloride ion, and several water solvate molecules. The Li^+ ion is located very close to the crystallographic 2-fold axis thus it has only half-occupancy. The Li^+ is coordinated by water molecules (two with full and one with half-occupancy), and the 2-fold symmetry axis gives rise to two tetrahedral cages (with water molecules on the tops) sharing one face, with a Li^+ ion occupying each cage by one-half. The chloride counterion is located very close to one water solvate molecule; thus, both fragments were refined as half-occupied. All non-hydrogen atoms were refined anisotropically. All hydrogen atoms were found in the electron density difference map, and were fixed in theoretical (C−H) or in original (N−H, O−H) positions.

Potentiometric Measurements. Potentiometric titrations were carried out to determine the protonation constants of the ligands and the stability constants of their complexes formed with selected metal ions at 1:1 metal-to-ligand molar ratio. Titrations were performed at 25.0 ± 0.1 °C and at an ionic strength of I = 0.1 M (NMe_4Cl) using deionized water. A constant passage of argon saturated with the solvent vapor provided the inert atmosphere. The initial volume in the titration vessel was 5 mL. Titrations were performed with NMe_4OH solution (∼0.2 M), and the concentration of the ligand was ∼0.004 M. For each determination, three parallel titrations were carried out, one titration consisting of about 50 points. All equilibria were established quickly. The titrations were run in the $-\log[H^+]$ range from 2 to 11.5 (or until precipitation of the metal hydroxide) with an extra HCl added to the starting solution employing a PHM 240 pH-meter, a 2-mL ABU 901 automatic piston buret and a GK 2401B combined electrode (all Radiometer, Denmark). In the Mn^{2+}-$H_2\mathbf{L^2}$ system, UV−vis spectra were recorded immediately after the potentiometric titration to exclude oxidation to Mn^{3+} species.

The OPIUM software package was used for calculations.[39,40] The value of pK_w was 13.81. Stability constants of the M^{2+}−OH^- systems were taken from literature.[41] For more details about potentiometric titrations, see previous papers.[42] In the following text, pH will mean $-\log[H^+]$ and all the equilibrium constants are concentration constants.

Dissociation Kinetics. The dissociation of $Mn\mathbf{L^1}$ was studied in the presence of Zn^{2+} followed by monitoring the relaxivity at 0.5 MHz on a Stelar SMARTracer Fast Field Cycling relaxometer (c_{Mn2+} = 1 mM, in 0.05 M *N*-methyl-piperazine buffer); in the pH range 5.1−6.2 and in the presence of 5, 10, 20, and 40-fold excess of the exchanging Zn^{2+} at 25 °C, 0.1 M KCl.

^{17}O NMR Measurements. Variable-temperature ^{17}O NMR measurements of aqueous solutions of the Mn^{2+} complexes (c_{MnL} = 5 mmol/kg, pH 8.0, in 0.1 M TRIS buffer; TRIS = tris-(hydroxomethyl)aminomethane) were performed on a Bruker Avance 500 MHz spectrometer (11.7 T, 67.8 MHz) in the temperature range 5−75 °C. The temperature was calculated according to previous calibration with ethylene glycol and MeOH.[43] Acidified water ($HClO_4$, pH = 3.3) was used as standard diamagnetic reference. The ^{17}O longitudinal (T_1) and transverse (T_2) relaxations times were obtained by the inversion−recovery pulse sequence[44] and Carl−Purcell−Meiboom−Gill spin-echo technique, respectively.[45] To eliminate the susceptibility corrections to the chemical shift,[46] the sample was placed in a glass sphere fixed in a 10-mm NMR tube. To improve sensitivity, the amount of ^{17}O was enriched by adding $H_2{}^{17}O$ (10% $H_2{}^{17}O$, CortecNet) to achieve approximately 1% ^{17}O content in the sample.

The variable-pressure ^{17}O NMR measurements were performed with the same solutions on a Bruker Avance-400 spectrometer (9.4 T, 54.2 MHz) equipped with a homemade high-pressure probe head in the pressure range 1−200 MPa.[47] The temperature (295 K) in the probe was regulated by circulating thermostatted ethanol through the probe and measured with a built-in Pt resistor. The sample was placed in a short 5-mm NMR tube closed with a special Teflon cylinder and then mounted in the high-pressure probe. Acidified water was used as a standard diamagnetic reference. The transverse (T_2) relaxation times were measured by the Carl−Purcell−Meiboom−Gill spin-echo technique.[45] The pressure dependence of the transverse relaxation rate of the acidified water, used as a reference, was described by assuming an activation volume of +0.97 $cm^3\ mol^{-1}$.[48]

^{1}H NMRD Measurements. The ^{1}H NMRD profiles of aqueous Mn^{2+} complex solutions (c_{Mn2+} = 5 mM, pH 8.0, 0.1 M TRIS buffer) were measured at 25 and 37 °C on a Stelar SMARTracer Fast Field Cycling NMR relaxometer (0.00024−0.24 T, 0.01−10 MHz ^{1}H Larmor frequency) and a Bruker WP80 NMR electromagnet adapted to variable-field measurements (0.47−1.88 T, 20−80 MHz ^{1}H Larmor frequency), and controlled by the SMARTracer PC-NMR console. The temperature was controlled by a VTC91 temperature unit and maintained by a gas flow. The temperature was determined according to previous calibration with a Pt resistance temperature probe.

Anion Binding Study. Relaxometric titrations were carried out on a Stelar SMARTracer Fast Field Cycling NMR relaxometer at 0.5 MHz and 25 °C to assess ternary complex formation with small endogenous anions. A solution of the anion ($c_{(phosphate)}$ = $c_{(carbonate)}$ = $c_{(citrate)}$ = 100 mM) was added stepwise to 1 mL of the Mn^{2+} complex solution (c_{Mn2+} = 1 mM, 0.1 M TRIS buffer, pH 8.0) up to 50 equiv of the anion.

Electrochemical Measurements. Cyclic voltammetric experiments were carried out on an Eco-Tribo Polarograph (ECOTrend Plus, Prague) driven by PolarPro 5.1 software. A conventional electrochemical three-electrode type cell was used with an Ag/AgCl reference electrode, a platinum wire auxiliary electrode, and a glassy carbon working electrode. The final potential values vs standard hydrogen electrode (SHE) were obtained using the relation between

Scheme 1. Reaction Scheme of the Preparation of the Protected Amine Precursors 1a and 1b[a]

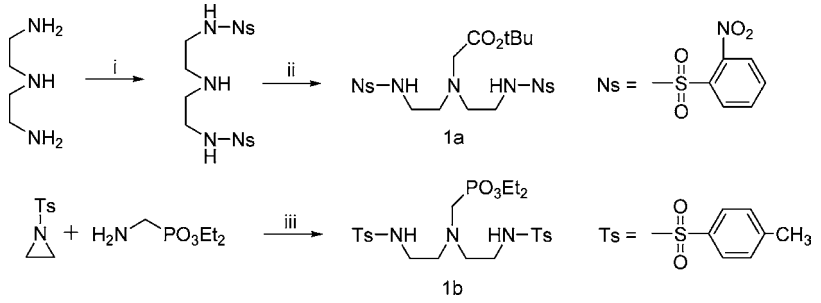

[a](i) NsCl, THF, RT 12 h; 69%; (ii) *t*-butyl bromoacetate, THF, Et_3N, 68%; (iii) toluene, reflux 12 h, 78%.

the two reference electrodes: Ag/AgCl electrode (sat. KCl) vs SHE = +198 mV. The measurements were performed in aqueous solutions in the presence of 0.05 M KCl (pH = 8.0 adjusted by KOH solution) as supporting electrolyte with a scan rate of 100 mV s^{-1} for 1 mM Mn^{2+} complex concentrations.

UV–vis Measurements. UV–vis spectra of aqueous Mn^{2+} complex solutions (c_{Mn2+} = 5 mM, pH 8.0, 0.1 M TRIS buffer) were recorded on a Varian Cary 5000 spectrophotometer (230–700 nm, at 25 °C) at different time intervals. The sample was placed in a 1-cm tempered double-wall cuvette and measured with a data interval of 2 nm.

Sample Preparation for NMR, Electrochemical, and UV–vis Measurements. Deoxygenated water was used to prepare all solutions, and all manipulations were done under Ar or N_2 atmosphere to prevent oxidation to Mn^{3+} by air. When the inert atmosphere was not guaranteed, several milligrams of hydroxylamine hydrochloride were added to prevent oxidation (no effect on the measured data). The Mn^{2+} complexes were prepared by mixing solutions of $MnCl_2$ and the ligand (25% ligand excess) and adjusting the pH with KOH or 0.1 M TRIS buffer to pH = 8.0.

Synthesis. *6-Carboxymethyl-3,6,9,15-tetraazabicyclo[9.3.1]-pentadeca-1(15),11,13-triene, HL*[1]. The protecting nosyl groups of **2a** were removed according to literature procedure.[49] The solution of *t*-butyl ester of the unprotected cycle (1.54 g, 4.81 mmol) in 100 mL of dichloromethane was cooled to 0 °C in water-ice bath, and trifluoroacetic acid (25 mL, 336 mmol) was added dropwise. The solution was stirred at room temperature for 12 h. Precipitated impurities were filtered off on a glass frit S4, and the solvent and the excess of trifluoroacetic acid were removed under reduced pressure. The residue was purified by flash silica gel chromatography (EtOH:NH_3 aq. 25% 10:1 to 1:1) and then on a cation exchange column (Dowex 50, H^+-form, 100 mL, elution with water and 15% aq. HCl) and an anion exchange column (Dowex 1 × 8, OH^--form, 150 mL, elution with water and 15% aq. HCl). The solvent was removed under reduced pressure, and the residue was dissolved in MeOH. The desired compound was obtained after evaporation of the MeOH solution as a yellow solid in the form of dihydrochloride (0.55 g, 34% yield).

NMR (D_2O+DCl). ^1H δ 3.14 (NCH_2CH_2NH, 4H, t, $^3J_{HH}$ = 5.4 Hz); 3.30 (NCH_2CH_2NH, 4H, t, $^3J_{HH}$ = 5.4 Hz); 3.78 (CH_2-C(O), 2H, s); 4.69 (NCH_2-py, 4H, s); 7.50 (CH arom., 1H, d, $^3J_{HH}$ = 8.1 Hz); 7.99 (CH arom., 2H, t, $^3J_{HH}$ = 8.1 Hz). $^{13}C\{^1H\}$ δ 48.8 (CH_2, 2C, s); 51.7 (CH_2, 2C, s); 55.3 (CH_2, 2C, s); 59.7 (CH_2, 1C, s); 124.7 (CH arom., 2C,s); 142.2 (CH arom., 1C, s); 151.3 (C arom., 2C,s); 177.4 (COOH, 1C, s). MS *m/z* (+): 264.8 $(L+H)^+$; 582.2 $(2\ L+H)^+$.

6-[(Dihydroxyphosphoryl)methyl]-3,6,9,15-tetraazabicyclo-[9.3.1]pentadeca-1(15),11,13-triene, H_2L^2. The solution of the ditosylated cycle **2b** (6.98 g, 10.5 mmol) dissolved in 98% H_2SO_4 (70 mL) was divided into 20-mL tubes each containing 1 mL of this solution. Each tube was heated to 70 °C then put in the 160 °C oil bath for exactly 90 s and left to cool to room temperature in air. The solutions from all tubes were collected in a 600-mL beaker and cooled with water-ice bath to 0 °C. The product precipitated as a hydrosulphate upon addition of diethylether (350 mL). The solid was decanted with diethylether (2 × 200 mL), dissolved in 10% aq. NH_3 (100 mL) and evaporated to dryness under reduced pressure. The residue was suspended in MeOH (25 mL), the undissolved solid was filtered off on a glass frit S3 and extracted with MeOH (3 × 10 mL). The collected filtrates were evaporated under reduced pressure, and the crude product was purified first on a cation exchange column (Dowex 50, H^+-form, 120 mL, elution with water and 15% aq. HCl) and then on an anion exchange column (Dowex 1 × 8, OH^--form, 150 mL, elution with water and 15% aq. HCl). The brown-yellow impurities were removed by 1 h reflux in water (50 mL) with activated charcoal which was filtered off on a glass frit S4. The filtrate was evaporated in vacuo, and the residue was dissolved in MeOH. The pure product was obtained after evaporation of the MeOH solution as a slightly yellow solid in form of dihydrochloride (2.81 g, 72% yield).

NMR (D_2O+DCl). ^1H δ 3.06 (NCH_2CH_2NH, 4H, t, $^3J_{HH}$ = 5.2 Hz); 3.21 (CH_2-P, 2H, d, $^2J_{PH}$ = 10.5 Hz); 3.34 (NCH_2CH_2NH, 4H, m); 4.68 (NCH_2-py, 4H, s); 7.49 (CH arom., 1H, d, $^3J_{HH}$ = 7.5 Hz); 7.99 (CH arom., 2H, t, $^3J_{HH}$ = 7.5 Hz). $^{13}C\{^1H\}$ δ 48.5 (CH_2, 2C, s); 52.3 (CH_2, 2C, s); 53.9 (CH_2, 1C, d, $^2J_{PH}$ = 151 Hz); 54.9 (CH_2, 2C, s); 124.8 (CH arom., 2C,s); 142.4 (CH arom., 1C, s); 151.3 (C arom., 2C,s). $^{31}P\{^1H\}$ δ 23.4 (s). MS *m/z* (+): 300.8 $(L+H)^+$; 601.2 $(2\ L+H)^+$; (−): 298.7 $(L-H)^-$; 599.1 $(2\ L-H)^-$.

RESULTS AND DISCUSSION

Synthesis. For the synthesis of both ligands, common amino-protecting groups were employed: 2-nitrobenzenesulfonyl (nosyl) for HL^1 and 4-methylbenzenesulfonyl (*p*-toluenesulfonyl, tosyl) for H_2L^2. The reaction pathways for the synthesis of both ligands via these two methods have been already described elsewhere;[32,33] however, these compounds were prepared as intermediates and were not isolated in free-acid forms. The protected precursors **1a** and **1b** were synthesized by literature procedures as shown in Scheme 1 using diethylenetriamine or tosylaziridine as starting compounds. In the preparation of **1a**, the nosyl chloride reacted preferentially with the primary amino groups of the diethylenetriamine ensuring the formation of dinosylated product with a free central secondary amino group which was modified by the (*t*-butoxycarbonyl)methyl group in the next reaction step. The ditosylated triamine with a phosphonate group, **1b**, was obtained in a good yield by the opening of the *N*-tosylaziridine ring in the presence of diethyl amino-methylphosphonate. The further reaction steps of the synthesis of HL^1 and H_2L^2 are shown in Scheme 2. The cyclization of the protected amines **1a** or **1b** and 2,6-bis(bromomethyl)pyridine was done in MeCN using K_2CO_3 as a base.[32] The pure cyclic products **2a** or **2b** were obtained after column chromatography on silica in good yields. The most problematic step was the deprotection. To efficiently remove the tosyl group, the solution of **2b** in concentrated sulfuric acid was heated to 160 °C but only in small volumes (1 mL) and for a short period

dx.doi.org/10.1021/ic201935r | *Inorg. Chem.* 2011, 50, 12785–12801

Scheme 2. Reaction Scheme ofthe Synthesis of Ligands HL^1 and H_2L^2 [a]

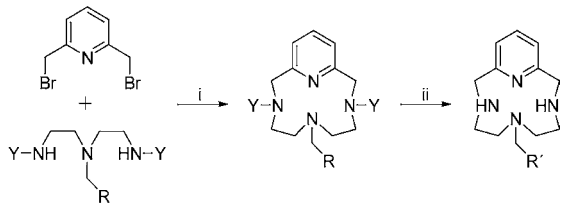

Y = Ns	**1a**	**2a**	HL^1
R = CO_2tBu		74%	34%
R′= COOH			
Y = Ts	**1b**	**2b**	H_2L^2
R = PO_3Et_2		78%	72%
R′= PO_3H_2			

Ns = nosyl. Ts = tosyl.

[a] HL^1 (i) K_2CO_3, MeCN, reflux 16 h; (ii) (a) PhSH, Na_2CO_3, DMF, RT 12 h; (b) TFA/CH_2Cl_2, RT 12 h; and H_2L^2: (i) K_2CO_3, MeCN, reflux 16 h; (ii) H_2SO_4 96%, 90 s at 160 °C.

of time (90 s) because longer heating led to the degradation of the phosphonate pendant arm resulting in 12-pyN_4 as main product. Aime et al. reported the same deprotection reaction[32] in 15 mL of the H_2SO_4 solution which was heated from 80 to 200 °C in 9 min but, in our hands, the reaction under such conditions was not successful. We also used the tosyl protecting group for the preparation of HL^1, but we were not able to find appropriate conditions for selective deprotection in H_2SO_4. The elevated temperature always induced decarboxylation and degradation of the pendant arm. Even at lower temperatures and short reaction times, the final mixture contained 12-pyN_4 or partially tosylated cycles with or without the pendant arm. Therefore we changed the protecting group from tosyl to nosyl which allows moderate conditions for the deprotection, typically RSH/DMF/base at room temperature (RT). The removal of the nosyl groups in **2a** by reaction with thiophenol and Na_2CO_3 in DMF at room temperature[33] was successful, and free HL^1 was obtained after the subsequent deesterification with TFA in CH_2Cl_2 (see Experimental Section).

Crystal Structures. As a byproduct formed in the first trials of the ligand synthesis, the nonderivatized macrocycle 12-pyN_4 was isolated. It crystallized as trihydrobromide (H_3-12-pyN_4)Br_3 in suitable form for X-ray diffraction analysis. The molecular structure of the $(H_3$-12-py$N_4)^{3+}$ cation (Figure 1) revealed that all three aliphatic amino groups are protonated in this triprotonated species, while the pyridine nitrogen atom is nonprotonated. This protonation scheme confirms the typical difference in basicity of the pyridine unit with respect to secondary aliphatic amines. The macrocycle conformation is rather irregular and stabilized by a medium-strong intramolecular hydrogen bond between the protonated amino group (N7) and the pyridine nitrogen atom ($d_{N\cdots N}$ ~2.8 Å, N–H···N angle 143°). The whole crystal structure is stabilized by a network of intermolecular hydrogen bonds between protonated amino groups and bromide anions (~3.2–3.6 Å).

The ligand H_2L^2 was successfully crystallized as the single crystal of $(H_4L^2)(H_3L^2)Br_3{\cdot}0.5H_2O$. Two independent ligand molecules were found in different protonation states. The first molecule is tetraprotonated, with a macrocyclic skeleton

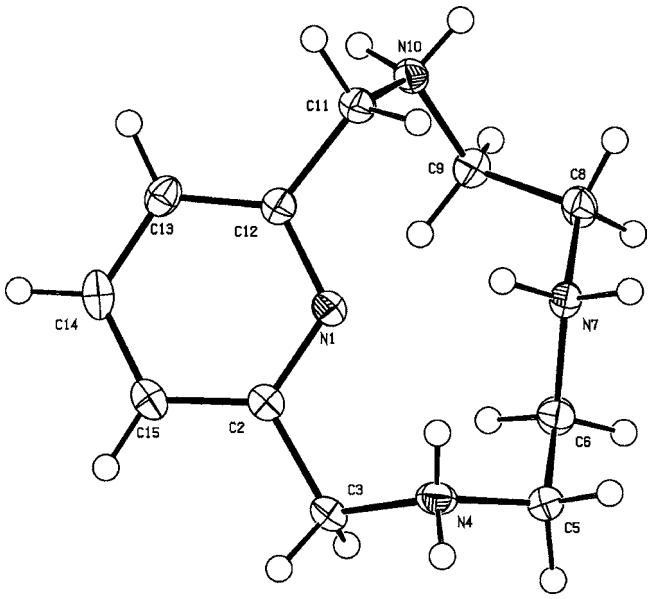

Figure 1. Molecular structure of the $(H_3$-12-py$N_4)^{3+}$ cation found in the crystal structure of (H_3-12-pyN_4)Br_3. The thermal ellipsoids are drawn with 50% probability.

diprotonated on two *trans* aliphatic amino groups, and two additional protons are attached to the phosphonate pendant moiety. The second molecule also has a diprotonated macrocyclic unit, but the phosphonate is only monoprotonated. In the independent molecules, the conformation of the two macrocyclic parts is very similar to each other and shovel-like, though the molecules differ in the position of the phosphonate moiety. In one of them, the double-protonated phosphonate (associated with the phosphorus atom P1, Figure 2) is turned away from the macrocycle, while in the other molecule (P51), it is turned above the macrocycle, participating in a rather weak intramolecular hydrogen bond system ($d_{O\cdots N}$ ~ 3.0 Å, N–H···O angles ~160°). The ligand molecules are connected via very strong intermolecular hydrogen bonds between protonated and nonprotonated phosphonate oxygen atoms ($d_{O\cdots O}$ ~2.44 and 2.49 Å, O–H···O angles ~165 and 174°, respectively), forming tetramer-like structures, which are further connected via the protonated oxygen atom O511 and the nonprotonated atom O13 from the neighboring tetramers ($d_{O\cdots O}$ ~2.56 Å, O–H···O angle ~171°). The bromide anions and water solvate molecules also participate in the hydrogen bond system, but via rather weak interactions.

From the $MnCl_2$–HL^1 aqueous mixture, single crystals of $[Mn(L^1)Cl]{\cdot}1.5H_2O$ suitable for an X-ray diffraction study were formed upon slow diffusion of acetone vapor. The manganese(II) ion is coordinated in a distorted octahedral fashion by four nitrogen atoms and one carboxylate oxygen atom of the macrocyclic ligand, and the last site is occupied by a chloride anion (Figure 3). This coordination mode confirms the expected possibility of water binding in aqueous solutions. The coordination bond between N(pyridine) and Mn is significantly shorter (~2.20 Å) as compared to the bonds to the aliphatic amino nitrogen atoms (~2.34–2.35 Å). The important geometrical parameters are listed in Table 2. The whole structure is stabilized by medium-strong hydrogen bonds between amino groups, water solvate molecules, and the coordinated chloride ion.

dx.doi.org/10.1021/ic201935r | *Inorg. Chem.* 2011, 50, 12785–12801

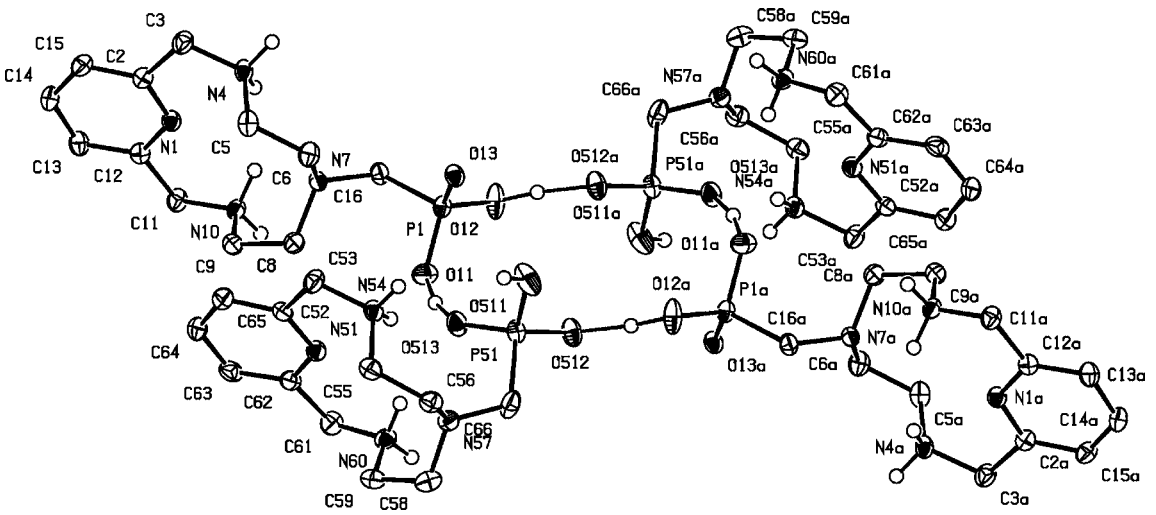

Figure 2. Part of the polymeric ligand structure found in the crystal structure of $(H_4\mathbf{L}^2)(H_3\mathbf{L}^2)Br_3{\cdot}0.5H_2O$. Hydrogen atoms bound to carbon atoms are omitted for clarity. The thermal ellipsoids are drawn with 50% probability.

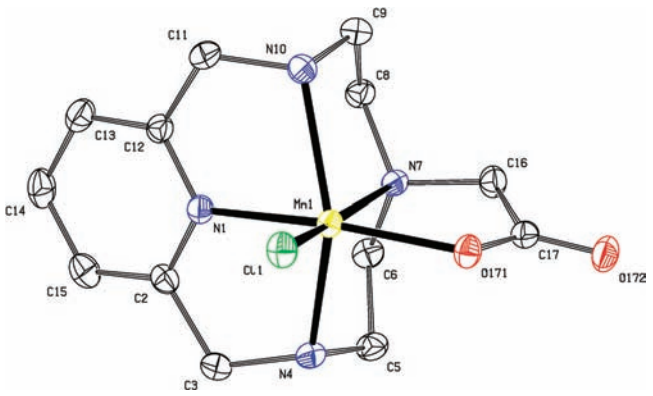

Figure 3. Molecular structure of $[Mn(\mathbf{L}^1)Cl]$ found in the crystal structure of $[Mn(\mathbf{L}^1)Cl]{\cdot}1.5H_2O$. The thermal ellipsoids are drawn with 50% probability. Hydrogen atoms are omitted for clarity.

For preparation of the single crystals of $[Mn(\mathbf{L}^2)]{\cdot}1/6NaCl{\cdot}1/3LiOH{\cdot}9H_2O$, slow diffusion of acetone vapor into the methanolic solution of $Mn(ClO_4)_2{-}H_2\mathbf{L}^2$ under argon atmosphere had to be used. The independent unit contains two complex species, which form two trimeric units because of a presence of a 3-fold rotational axis. The complex units in the trimer are connected to each other via bridging coordination of one of the phosphonate oxygen atoms. One of these trimers (three phosphonate oxygen atoms) is templated by Na^+ ion (laying on the 3-fold axis), whose coordination sphere is closed by three water molecules forming a distorted octahedron (Figure 4a), and Li^+ ion with an apically coordinated (probably) hydroxide anion. The other trimeric unit is turned around the electronic maximum, which was also attributed to Li^+ ion because of the corresponding intensity and bonding distances (Figure 4b). Its coordination sphere is closed by one oxygen atom originating probably from a hydroxide anion. The manganese(II) ions are coordinated in a distorted octahedral fashion, with four nitrogen atoms and one phosphonate oxygen atom coming from the macrocyclic ligand and the last site occupied by a phosphonate oxygen atom from the neighboring molecule. The important geometrical parameters are listed in Table 2, and they fully support the formulation as a divalent manganese complex.

Using the previous procedure with crystallization open to air, the manganese(II) oxidized to manganese(III), and single crystals of $[Mn(\mathbf{L}^2)(OH)]{\cdot}0.5LiCl{\cdot}7H_2O$ were isolated. The manganese(III) ion is coordinated in a distorted octahedral fashion, with four nitrogen atoms and one phosphonate oxygen atom coming from the macrocyclic ligand and the last site is occupied by a hydroxide anion (Figure 5). The trivalency of the central manganese(III) ion is evidenced from coordination distances which are significantly shorter than those for the previous manganese(II) complexes, as the consequence of a shorter ionic radius. The metal ion fits better into the macrocyclic cavity resulting in more regular bond angles, though the coordination polyhedron remains distorted. The important geometrical parameters are listed in Table 2.

Equilibrium Studies. The protonation constants of the ligands as well as the thermodynamic stability constants of their complexes with Mn^{2+} and selected divalent metal ions were determined by potentiometry. The protonation constant of $H\mathbf{L}^1$ and $H_2\mathbf{L}^2$ together with those previously reported for some relevant macrocyclic ligands are listed in Table 3 (for a complete data set with standard deviations see Supporting Information, Table S1). For the 12-membered pyridine-based macrocycles, the functionality in the pendant arm has an important influence on the first protonation constant; log K_{H1} increases in the order 12-pyN_4 (no pendant arm) < $H\mathbf{L}^1$ (one acetate) < $H_2\mathbf{L}^2$ (one phosphonate) resulting in a higher ligand basicity. This is in a good correlation with the increasing positive inductive effect of carboxylate and fully deprotonated phosphonate groups previously observed for analogous ligands.[50] Basicity increase is observed also upon the stepwise introduction of acetate pendant arms on the secondary amino groups: log K_{H1} increases from 12-pyN_4 to $H\mathbf{L}^1$ and to PC2A, but it finally drops for PCTA.

The protonation sequence of both ligands studied was assessed by ^{1}H NMR titration. The variable pH ^{1}H NMR titration is well established for polyaminocarboxylates/phosphonates when the protonation of a basic site results in a deshielding of the resonance of the adjacent nonlabile protons in the ^{1}H NMR spectrum. The ^{1}H NMR titration data with the indication of the protonation constants as obtained from potentiometry (solid lines) are shown in Figure 6. For $H\mathbf{L}^1$ between pH 12–8, all proton signals have a downfield shift

dx.doi.org/10.1021/ic201935r | Inorg. Chem. 2011, 50, 12785–12801

Table 2. Selected Geometrical Parameters Found for the Manganese Complexes Studied

parameter	$[Mn(L^1)Cl]\cdot 1.5H_2O$	$[Mn(L^2)]\cdot 1/6NaCl\cdot 1/3LiOH\cdot 9H_2O$		$[Mn(L^2)(OH)]\cdot 0.5LiCl\cdot 7H_2O$
unit	$[Mn(L^1)Cl]$	$\{Na(H_2O)_3[Mn(L^2)]_3Li(OH)\}^+$	$\{Li(OH)[Mn(L^2)]_3\}$	$[Mn(L^2)(OH)]$
		Distances		
Mn1−N1	2.199(1)	2.192(6)	2.229(5)	2.068(2)
Mn1−N4	2.341(1)	2.310(6)	2.322(4)	2.295(2)
Mn1−N7	2.350(1)	2.378(5)	2.332(5)	2.142(2)
Mn1−N10	2.335(1)	2.301(5)	2.359(5)	2.278(2)
Mn1−O(pendant)	2.122(1)	2.092(4)	2.119(4)	1.920(1)
Mn1−X	2.429(1)[a]	2.100(4)[b]	2.082(4)	1.836(1)[c]
		Angles		
N1−Mn1−N4	73.99(5)	73.8(2)	71.1(2)	76.94(6)
N1−Mn1−N7	86.02(5)	87.1(2)	99.9(2)	89.27(6)
N1−Mn1−N10	74.22(5)	74.5(2)	72.4(2)	76.93(6)
N1−Mn1−O(pendant)	159.28(5)	169.0(2)	173.3(2)	174.14(6)
N1−Mn1−X	101.44(4)[a]	94.6(2)[b]	89.2(2)[b]	93.31(6)[c]
N4−Mn1−N7	78.33(5)	77.9(2)	77.2(2)	81.32(6)
N4−Mn1−N10	140.76(5)	140.1(2)	131.1(2)	148.26(6)
N4−Mn1−O(pendant)	91.52(5)	101.7(2)	115.4(2)	98.09(6)
N4−Mn1−X	109.40(4)[a]	103.2(2)[b]	95.6(2)[b]	101.26(6)[c]
N7−Mn1−N10	77.11(5)	76.9(2)	78.3(2)	80.65(6)
N7−Mn1−O(pendant)	76.42(5)	82.1(2)	80.4(2)	86.89(6)
N7−Mn1−X	170.39(4)[a]	178.2(2)[b]	165.7(2)[b]	176.70(6)[c]
N10−Mn1−O(pendant)	111.63(5)	104.8(2)	101.2(2)	106.75(6)
N10−Mn1−X	98.94(4)[a]	103.0(2)[b]	115.3(2)[b]	97.93(6)[c]
O(pendant)−Mn1−X	97.28(3)[a]	96.2(2)[b]	91.8(2)[b]	90.69(6)[c]
		Dihedral Angles−Macrocyclic Conformation		
N1−C2−C3−N4	−20.1(2)	18(1)	30.7(7)	−22.9(2)
N4−C5−C6−N7	60.8(2)	−61.2(9)	57.7(6)	58.0(2)
N7−C8−C9−N10	−56.3(2)	57.3(7)	56.0(6)	−58.1(2)
N10−C11−C12−N1	26.4(2)	−26(1)	−19.7(8)	23.4(2)

[a]Chloride ion. [b]Oxygen atom from neighboring molecule. [c]Hydroxido ligand.

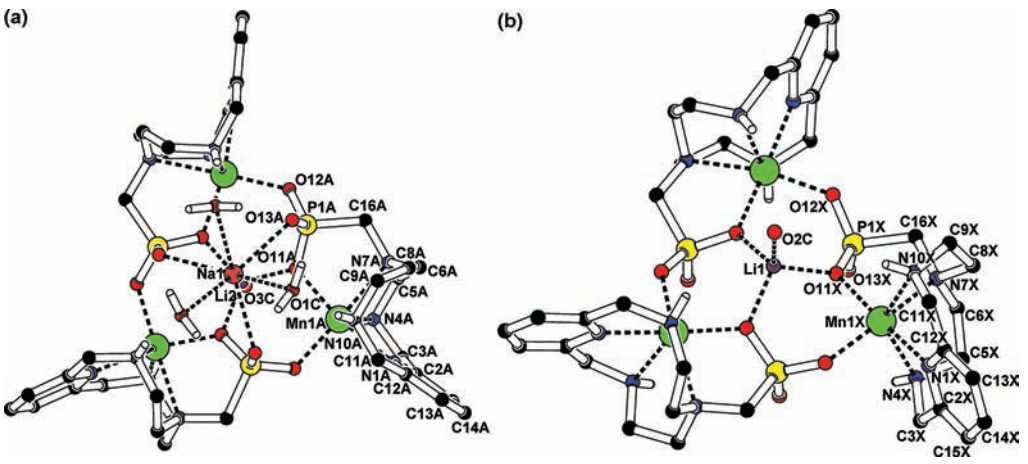

Figure 4. Trimeric unit $\{Na(H_2O)_3[Mn(L^2)]_3Li(OH)\}^+$ (a) and $\{Li(OH)[Mn(L^2)]_3\}$ (b) found in the crystal structure of $[Mn(L^2)]\cdot 1/6NaCl\cdot 1/3LiOH\cdot 9H_2O$. The thermal ellipsoids are drawn with 50% probability. Hydrogen atoms on carbon atoms are omitted for clarity.

corresponding to the addition of two protons (log K_{H1} = 10.47, log K_{H2} = 8.71). The largest shift of the CH_2 resonances 2/10 and 4/8 (for numbering, see Figure 7) indicate the protonation of the secondary amino groups. Since the CH_2 protons 5/7 display an analogous change while protons 16 have a smaller downfield shift in the same pH region, it is reasonable to suppose some positive charge on N6 and thus some charge transfer from N6 to N3 or N9 may occur to form a species diprotonated on N3 and N9 with the lowest electrostatic repulsion between the two ammonium groups. This observation is in agreement with the higher values of the first two protonation constants of HL^1 in comparison to those of 12-pyN_4 which can be explained by a positive inductive effect of the carboxylate and/or hydrogen bonding between the carboxylate and the protonated ring nitrogen atoms. The small downfield shift of the proton resonance 16 between pH 2−4 corresponds to the last protonation step (log K_{H3} = 2.79) that occurs on the acetate group.

A similar protonation sequence was found for H_2L^2 where the pH dependency of the ^{31}P NMR shifts was also monitored. Between pH 10.5−13, the largest downfield shift

dx.doi.org/10.1021/ic201935r | Inorg. Chem. 2011, 50, 12785−12801

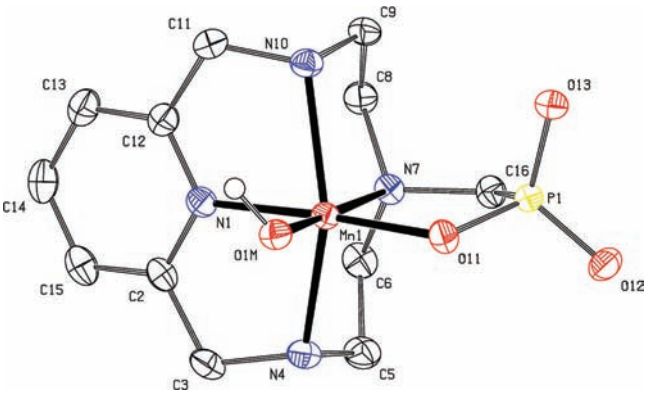

Figure 5. Molecular structure of $[Mn(L^2)(OH)]$ found in the crystal structure of $[Mn(L^2)(OH)]\cdot 0.5LiCl\cdot 7H_2O$. The thermal ellipsoids are drawn with 50% probability. Hydrogen atoms (except coordinated OH^- group) are omitted for clarity.

Table 3. Stepwise Protonation Constants[a] of HL^1, H_2L^2, and Other Relevant Ligands Obtained from Potentiometry (25 °C, I = 0.1 M)[b]

	log K_{H1}	log K_{H2}	log K_{H3}	log K_{H4}
HL^1	10.47(1) [10.53(5)]	8.71(2) [9.10(10)]	2.79(2) [2.82(11)]	
H_2L^2	11.84(1) [11.54(3)]	9.64(1) [9.66(1)]	6.23(1) [6.19(2)]	0.99(2) [0.57(3)]
12-pyN_4[c]	10.33	7.83	1.27	<1
PC2A[d]	12.5	5.75	3.28	2.38
PCTA[e]	10.90	7.11	3.88	2.27
15-pyN_3O_2[f]	8.82	7.80		
15-pyN_5[f]	9.40	8.54	5.28	
9-aneN_2O-2A[g]	10.57	4.02	1.80	
9-aneN_2O-2P[g]	12.32	7.88	5.43	1.86

[a]Defined as $K_{Hi} = [H_iL]/[H^+] \times [H_{i-1}L]$ for i = 1−4 (charges were omitted for clarity). [b]The values in brackets were calculated from pH-NMR titrations. [c]I = 0.1 M KNO_3, ref 51. [d]Ref 52. [e]Ref 53. (I = 0.1 M KNO_3). [f]Ref 27. [g]Ref 28.

occurs on the methylene protons 5/7 and 16 indicating protonation of the most basic tertiary N6. This step, corresponding to the first protonation constant log K_{H1} = 11.84, is confirmed by an upfield shift of the ^{31}P NMR resonance of the phosphonic acid group, as it has been already observed for similar cyclic amines with phosphonate pendant arm(s).[54] The next protonation in the pH range 8−10.5, with log K_{H2} = 9.64, leads to a relocalization of protons to the secondary amino groups (N3 and N9). This is indicated by a small upfield shift of protons 5/7 and 16 whereas all the others are more deshielded. This proton transfer is also confirmed by the complete recovery of the ^{31}P chemical shift at pH ∼8 resulting in a diprotonated species showing the lowest electrostatic repulsion between the ammonium N3 and N9 nitrogen atoms. The next two protonation steps between pH 5−7 and 0−2, corresponding to log K_{H3} = 6.23 and log K_{H4} = 0.99, occur on the oxygen atoms of the phosphonate group as evidenced by the constant shifts of the CH_2 protons (except resonance 16) and the two downfield shifts of the ^{31}P NMR signal.

A strong line-broadening of the ring CH_2 resonances in ^1H NMR is observed for the mono- and diprotonated forms of HL^1 and H_2L^2. These resonances became sharp for the unprotonated forms while the methylene resonances of the

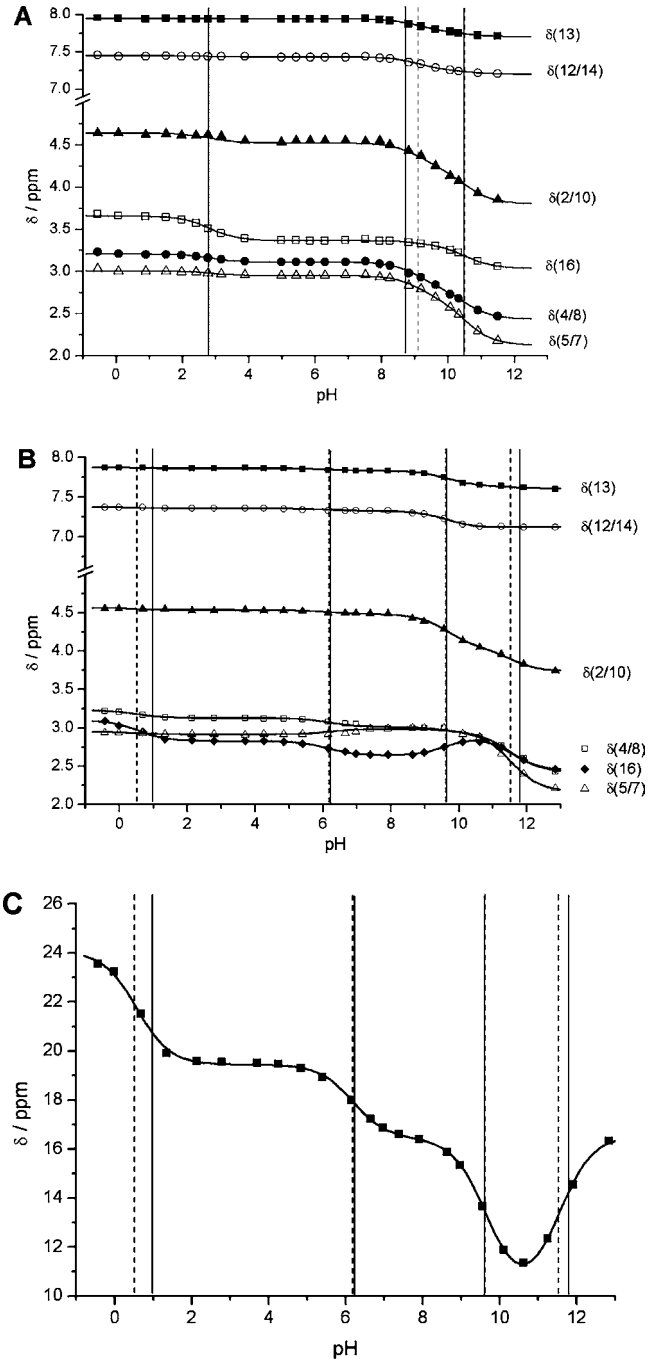

Figure 6. pH dependence of ^1H NMR resonances of HL^1 (a) and H_2L^2 (b) and pH dependent ^{31}P shifts of H_2L^2 (c). The solid and the dashed vertical lines represent the log K_{Hi} values obtained from potentiometry and from pH-NMR titrations, respectively.

pendant arm remain unaffected upon deprotonation. A similar phenomenon has been described by Geraldes et al. for macrocyclic triazatriacetates,[55] where the line-broadening was attributed to a slow interconversion between the various ring conformations because of a slow nitrogen inversion in the partially protonated forms. It was suggested that such a slow nitrogen inversion originates from intramolecular hydrogen bonding between the protonated nitrogen atoms and the carboxylates. Because of their similar structure, the same reasoning may apply to HL^1 and H_2L^2 as well. Similar slow interconversion was observed for phenylphosphinic acid

dx.doi.org/10.1021/ic201935r | Inorg. Chem. 2011, 50, 12785−12801

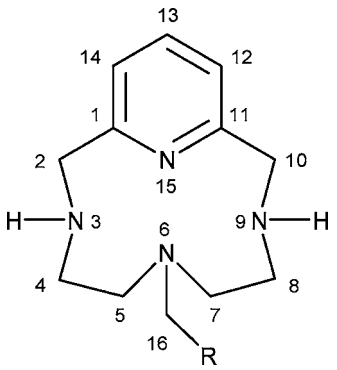

Figure 7. Numbering scheme of HL^1 (R = CO_2H) and H_2L^2 (R = PO_3H_2).

analogues of DOTA and TETA causing line broadening in the ^{31}P NMR spectra.[56]

The stability constants of the complexes formed with Mn^{2+} and selected divalent metal ions as determined by potentiometry are listed in Table 4 (for the complete data set with standard deviations, see Supporting Information, Table S1). Monoprotonated complexes as well as mono- and dihydroxido species were found in the systems studied. Mg^{2+} and Ca^{2+} form weak complexes with both ligands, and there is a small selectivity of H_2L^2 for Mg^{2+} with respect to Ca^{2+}. A similar preference for Mg^{2+} has been already observed for phosphorus-containing derivatives of NOTA.[57] According to the Irwing–Williams rule, Mn^{2+} forms the less and Cu^{2+} the most stable complexes with both ligands among the investigated transition metal ions. Indeed, the stability constants are 7–8 orders of magnitude higher for the Cu^{2+} than for the Mn^{2+} complexes, and Zn^{2+} also forms very stable complexes in comparison with Mn^{2+}. The distribution diagrams for Mn^{2+}–HL^1 (A) and Mn^{2+}–H_2L^2 (B) systems are depicted in Figure 8. They show the complete complex formation above physiological pH = 7.4. The stability constants of various Mn^{2+} complexes are compared in Table 5. The stability can be also easily assessed by the percentage of free noncomplexed Mn^{2+} at pH 7.4 in systems with equimolar concentration of metal and ligand ($c_{Mn2+} = c_L$ = 5 mM or with 2-fold ligand excess (c_{Mn2+} = 5 mM, c_{lig} = 10 mM). The pMn values were also calculated for conditions commonly used for Gd^{3+} chelates (pH = 7.4, $c_{Mn2+} = 10^{-6}$ M, $c_{lig} = 10^{-5}$ M). The low percentage of free Mn^{2+} and the high pM values evidence a reasonable thermodynamic stability of MnL^1 and MnL^2 (Table 5). Nevertheless, the thermodynamic stability is comparable only to that of the EDTA analogue and still lower than those of complexes with hexadentate (or higher denticity) ligands like PCTA, NOTA, or DOTA.

For Gd^{3+} complexes of different linear or cyclic polyaminocarboxylates/phosphonates, a linear relationship has been reported between the experimentally measured log K_{ML} and $\sum$ log K_{Hi} values. We checked this relationship for Mn^{2+} complexes of HL^1, H_2L^2, and other cyclic ligands. Usually, $\sum$ log K_{Hi} represents the sum of all protonation constants that result in a neutral ligand. Here, for a comparison also involving neutral ligands, we included only the first two protonation constants. Figure 9 confirms the linear dependency of log K_{ML} on $\sum$ log K_{Hi} (i = 1, 2). As expected, the most basic 12-membered ligands HL^1 and H_2L^2 result in the highest stability constants for the Mn^{2+} complex.

Kinetic Inertness. In addition to thermodynamic stability, kinetic inertness is another important parameter for safe in vivo application of a Mn^{2+} complex as an MRI CA. The complex needs to be sufficiently inert under in vivo conditions toward proton-catalyzed dissociation or transmetalation by endogenous ions such as Ca^{2+}, Cu^{2+}, or Zn^{2+} because free Mn^{2+} and free ligand are both toxic. The in vivo release of Mn^{2+} from the thermodynamically stable $[Mn(dtpa)]^{3-}$ was observed[13] and, in general, Mn^{2+} complexes were believed to be kinetically labile.

Table 4. Stability Constants[a] of H_2L^1 and H_2L^2 Complexes with Selected Metal Ions[b]

constant[a]	Mg^{2+}	Ca^{2+}	Mn^{2+}	Zn^{2+}	Cu^{2+}
		HL^1			
log K_{LM}	6.37	6.04	11.54	17.01	18.62
log K_{HLM}	7.34	7.39	4.95	3.03	2.09
log $K_{LM(OH)}$	11.2			10.46	11.35
log $K_{LM(OH)2}$	12.33				
		H_2L^2			
log K_{LM}	8.29	6.85	14.06	19.66	22.63
log K_{HLM}			5.35	5.19	4.89
log $K_{LM(OH)}$	12.31		−11.97	12.33	13.12
log $K_{LM(OH)2}$	11.96				

[a]Defined as $K_{ML} = [ML]/[M] \times [L]$; $K_{ML(OH)i} = [ML(OH)_i] \times [H^+]/[ML(OH)_{i-1}]$, for i = 1, 2; $K_{HML} = [HML]/[ML] \times [H^+]$. [b]25 °C, I = 0.1 M NMe_4Cl.

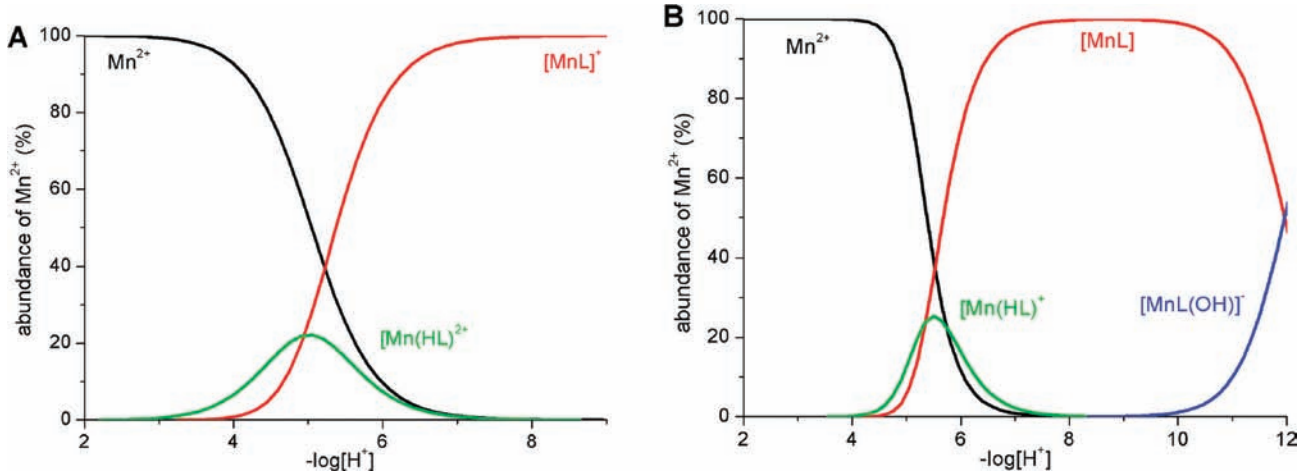

Figure 8. Distribution diagrams for Mn^{2+}–HL^1(A) and Mn^{2+}–H_2L^2 (B) systems ($c_{Mn2+} = c_L$ = 4 mM, I = 0.1 M NMe_4Cl).

dx.doi.org/10.1021/ic201935r | Inorg. Chem. 2011, 50, 12785–12801

Table 5. Stability Constants,[a] Percentage of Non-Complexed Mn^{2+} [b] and pMn[c] Values for Mn^{2+} Complexes

	HL[1]	H_2L^2	15-pyN_3O_2[d]	15-pyN_5[d]	9-aneN_2O-2A[e]	9-aneN_2O-2P[e]
log K_{LM}	11.54	14.06	7.18	10.89	7.43	10.61
log K_{HLM}	4.95	5.35		4.27		6.32
log $K_{LM(OH)}$		−11.97	−11.69	−11.52	−10.85	−12.42
(a) % free Mn^{2+}	0.37	0.29	3.45	0.12	10.2	3.89
(b) % free Mn^{2+}	1.3×10^{-3}	8.3×10^{-4}	0.12	3.8×10^{-4}	1.13	0.16
pMn[c]	8.10	8.30	6.40	8.67	6.07	6.34

	12-pyN_4[f]	PCTA[g]	EDTA[h]	NOTA[h]	DOTA[h]
log K_{LM}	8.81	18.59	13.88	16.30	19.89
log K_{HLM}		2.21		2.87	4.26
log $K_{LM(OH)}$		8.71			2.99
(a) % free Mn^{2+}	3.07	4.96×10^{-5}	4.40×10^{-3}	7.8×10^{-3}	3.60×10^{-4}
(b) % free Mn^{2+}	9.73×10^{-2}	2.46×10^{-11}	1.93×10^{-7}	6.0×10^{-7}	1.30×10^{-9}
pMn[c]	6.46	15.86	11.97	11.47	14.14

[a]Defined as $K_{ML} = [ML]/[M] \times [L]$; $K_{ML(OH)} = [ML(OH)] \times [H^+]/[ML]$; $K_{HML} = [HML]/[ML] \times [H^+]$. [b]pH = 7.4, for (a) $c_{Mn2+} = c_{lig} = 5$ mM or for (b) $c_{Mn2+} = 5$ mM, $c_{lig} = 10$ mM. [c]pMn = $-\log[Mn^{2+}_{free}]$ for pH = 7.4, $c_{Mn2+} = 10^{-6}$ M, $c_{lig} = 10^{-5}$ M. [d]Ref 27. [e]Ref 28. [f]Ref 50. [g]Ref 52. [h]Ref 41.

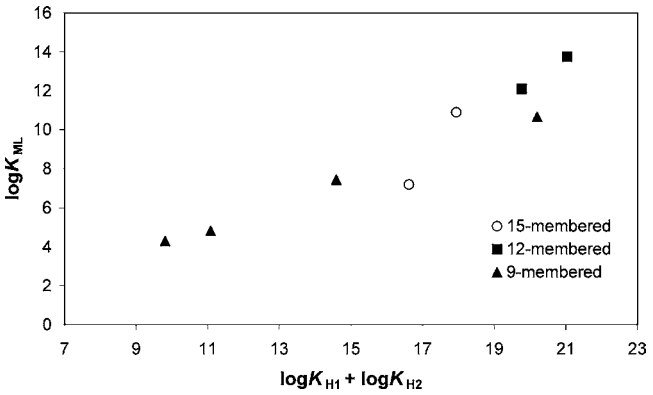

Figure 9. Dependency of MnL stability constants on the sum of the first two protonation constants of the ligand containing 15-membered (15-pyN_3O_2 and 15-pyN_5), 12-membered (HL^1 and H_2L^2) and 9-membered macrocyclic rings (9-aneN_2O-2P^H, 9-aneN_2O-2P^{Ph}, 9-aneN_2O-2A, 9-aneN_2O-2P).

Recently, we have investigated the dissociation of Mn^{2+} complexes with NOTA and DOTA. The results revealed unexpectedly high kinetic inertness. The Mn(15-pyN_5) complex showed faster dissociation, related to the presence of two inner-sphere water molecules and to the more "open" structure of the complex.

Here we followed the dissociation kinetics of MnL^1 and MnL^2 under the experimental conditions typically used in studies of Gd^{3+} chelates. The reaction between the Mn^{2+} complex and the diamagnetic Zn^{2+} at various concentrations of the exchanging ion and pHs was monitored by relaxometry. The relaxivity increase in time is the result of the release of free Mn^{2+} by Zn^{2+} transmetalation or proton-assisted complex dissociation. For MnL^1, the observed dissociation rate constants in the pH range 5.1−6.2 and in the presence of 5−50-fold excess of Zn^{2+} are reported in Figure 10 and Supporting Information, Table S2. The dissociation of MnL^2 was too fast to be followed under similar experimental conditions despite the higher thermodynamic stability of MnL^2. The higher abundance of the protonated species at pH 6 and the higher basicity of H_2L^2 are probably responsible for the very fast proton-assisted dissociation of the complex. Above pH 6.2, the complexation of Zn^{2+} by the phosphonate groups resulting in oligomers or polymers and the partial hydrolysis of $[Zn(H_2O)_6]^{2+}$ prevented the measurements.

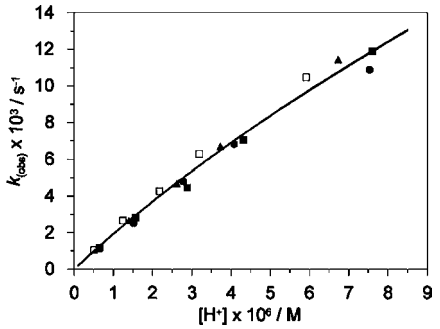

Figure 10. Dependence of the observed dissociation rate constants for MnL^1 on the proton concentration at Zn^{2+} concentrations of 5 mM (■), 10 mM (●), 20 mM (▲), and 40 mM (□). The line corresponds to the best fit with the parameters given in Table 4.

The excess of the exchanging metal ion ensures that the reaction rate is directly proportional to the total concentration of MnL^1 and thus the reaction is of pseudo-first order, as given in eq 1, where k_{obs} is the pseudo-first-order rate constant.

$$-\frac{d[MnL]_{tot}}{dt} = k_{obs}[MnL]_{tot} \quad (1)$$

In general, the dissociation can proceed via different pathways, as illustrated in Scheme 3. The overall rate of the exchange reaction can be thus given by eq 2 (in the equations, charges of the complexes are omitted for clarity).

Scheme 3. Possible Dissociation Pathways for MnL^1[a]

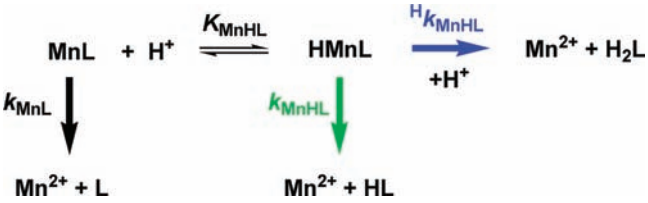

[a]Charges of ligand and complex species are omitted for clarity.

$$-\frac{d[MnL]_{tot}}{dt} = k_{MnL}[MnL] + k_{MnHL}[MnHL] + {}^{H}k_{MnHL}[MnHL][H^+] \quad (2)$$

dx.doi.org/10.1021/ic201935r | Inorg. Chem. 2011, 50, 12785−12801

Table 6. Parameters Characterizing the Dissociation Kinetics of Mn^{2+} Complexes with H_2L^1 and Some Previously Studied Ligands and $[Gd(dtpa)(H_2O)]^{2-}$

parameters	H_2L^1	15-pyN$_5$[a]	NOTA[b]	DOTA[b]	$[Gd(dtpa)(H_2O)]^{2-}$ [c]
k_0/s^{-1}			2.6×10^{-6}	1.8×10^{-7}	
$k_1/M^{-1}\ s^{-1}$	2020 ± 40	423	7.8×10^{-1}	4.0×10^{-2}	0.58
$k_2/M^{-2}\ s^{-1}$	$(8.0 \pm 0.3) \times 10^7$	1.0×10^7		1.6×10^3	9.7×10^4
$k_3/M^{-1}\ s^{-1}$			1.1×10^{-5}	1.5×10^{-5}	5.6×10^{-2}
$k_4/M^{-2}\ s^{-1}$		1.7×10^4			
log K_{MHL}	4.95	4.27	2.87	4.26	2
log K_{MH2L}				2.99	
K_{MnLZn}			3.6	68	$K_{GdLZn} = 7$
$t_{1/2}$ (pH 6.0, $c(Zn^{2+}) = 10^{-3}$ M)	6 min	26 min	58 h	868 h	3.42 h
$t_{1/2}$ (pH 6.0, $c(Zn^{2+}) = 10^{-5}$ M)	6 min	27 min	58 h	869 h	156 h
$t_{1/2}$ (pH 7.4, $c(Zn^{2+}) = 10^{-3}$ M)	144 min	11.0 h	74 h	1024 h	3.46 h
$t_{1/2}$ (pH 7.4, $c(Zn^{2+}) = 10^{-5}$ M)	144 min	11.4 h	74 h	1037 h	330 h

[a]Ref 27. [b]Ref 14. [c]Ref 58.

Here, the first term corresponds to the spontaneous dissociation of the complex, the second one to the spontaneous dissociation of the protonated complex, and the last term to the proton-assisted dissociation of the protonated complex. If we consider the total complex concentration as in eq 3

$$[MnL]_{tot} = [MnL] + [MnHL] \quad (3)$$

the pseudo-first-order rate constant, k_{obs}, is defined by eq 4

$$k_{obs} = \frac{k_0 + k_1[H^+] + k_2[H^+]^2}{1 + K_{MnHL}[H^+]} \quad (4)$$

where $k_0 = k_{MnL}$, $k_1 = k_{MnHL} \cdot K_{MnHL}$, $k_2 = {}^{H}k_{MnHL} \cdot K_{MnHL}$.

The experimental rate constants were fitted to eq 4, and the calculated parameters are compared with those obtained for other Mn^{2+} chelates and $[Gd(dtpa)]^{2-}$ in Table 6. The protonation constant of Mn**L**^{1}, K_{MnHL}, was obtained from potentiometry and fixed to log $K_{MnHL} = 4.95$. During the fitting procedure, we obtained a small negative value for k_0 and therefore it was fixed to zero. Thus, the spontaneous dissociation of Mn**L**^{1} does not contribute to the overall dissociation. The rate constants k_1 and k_2 corresponding to the spontaneous and proton-assisted dissociation of the protonated complex MnH**L**^{1} were calculated. Other possible dissociation pathways involving the dissociation of the dinuclear Mn^{2+}-**L**^{1}-Zn^{2+} complex (k_3) or zinc-assisted dissociation of the protonated complex (k_4) were also taken into account (for a full set of equations used in the fit see Supporting Information), but their influence on the overall dissociation was negligible. Among the various complexes compared, Mn**L**^{1} has the fastest overall dissociation, related to the highest rate constant of the spontaneous dissociation of the protonated complex, k_1. The value of k_1 is 5-times higher for Mn**L**^{1} than for 15-pyN$_5$ while for MnNOTA and MnDOTA it is 3−4 orders of magnitude lower. The proton-assisted dissociation of the protonated complex, characterized by k_2, does not have a strong influence; its contribution to the overall dissociation at the highest proton concentration is 23%. The value of k_2 is comparable to that for 15-pyN$_5$, and it is several orders of magnitude higher than that for MnDOTA. For the previously reported Mn^{2+} complexes, Zn^{2+} either enhanced (Mn15-pyN$_5$) or suppressed (MnDOTA, MnNOTA) the dissociation. Here, the increasing Zn^{2+} concentration has no influence on the overall dissociation rate. To estimate the dissociation under in vivo conditions and to better compare all complexes, we calculated the dissociation half-times for physiological pH and Zn^{2+} concentration (Table 6).

^{17}O NMR and ^{1}H NMRD. The effect of paramagnetic species to enhance the nuclear relaxation processes is described by the Solomon−Blombergen−Morgan theory of paramagnetic relaxation.[4] The microscopic parameters governing the relaxivity are commonly calculated using this model. ^{1}H NMRD profiles, representing the magnetic field dependence of relaxivity are crucial to assess these parameters and to distinguish between different relaxation mechanisms. A large number of parameters influence the ^{1}H NMRD profiles and therefore some of them are usually determined by independent techniques, like ^{17}O NMR. The variable-temperature ^{17}O transverse relation rates ($1/T_2$) provide direct access to the water exchange rate, k_{ex}, (water residence time $\tau_M = 1/k_{ex}$) while the longitudinal relaxation rates ($1/T_1$) carry information about the rotational motion of the molecule, described by the rotational correlation time, τ_R. The temperature dependency of the ^{17}O chemical shifts (ω) informs about the hydration number (q) of the complex.

The variable-temperature transverse ^{17}O relaxation times and chemical shifts were measured on aqueous solution of Mn**L**^{1} and Mn**L**^{2} at pH 8 with 10% ligand excess to ensure full complex formation (Figure 11). The longitudinal relaxation times were also measured, but they were not included in the treatment of the ^{17}O NMR data because the difference between the complex solution and the diamagnetic reference was too small (3−5%) giving large errors in the reduced relaxation rates. ^{1}H NMRD profiles were measured at 25 and 37 °C in the magnetic field range 0.01−80 MHz (Figure 12). The ^{1}H NMRD profiles were analyzed simultaneously with the ^{17}O NMR data (see Supporting Information for equations used for the simultaneous fitting); the fitted parameters are shown and compared to those of other Mn^{2+} chelates and $[Mn(H_2O)_6]^{2+}$ in Table 7.

The temperature dependency of the ^{17}O transverse relaxation rates and the chemical shifts ω shows that both systems are in the fast water exchange regime. We should note that the contribution of the electronic relaxation to the ^{17}O transverse relaxation rates is negligible (<1% in the correlation time $1/\tau_s = k_{ex} + 1/T_{1e}$ under the experimental conditions). The calculated water exchange rate constants are extremely high; $k_{ex}^{298} = 3.04 \times 10^9\ s^{-1}$ for Mn**L**^{1} is the highest value ever measured and is about 2-times higher than that for Mn**L**^{2}. The Mn^{2+} complex of 9-aneN$_2$O-2A has a water exchange rate about twice as low, $k_{ex} = 1.19 \times 10^9\ s^{-1}$,[28] similar to that for $[Mn(nta)(H_2O)_2]^-$ ($k_{ex} = 1.5 \times 10^9\ s^{-1}$).[61] Apart from these few chelates, the

dx.doi.org/10.1021/ic201935r | Inorg. Chem. 2011, 50, 12785−12801

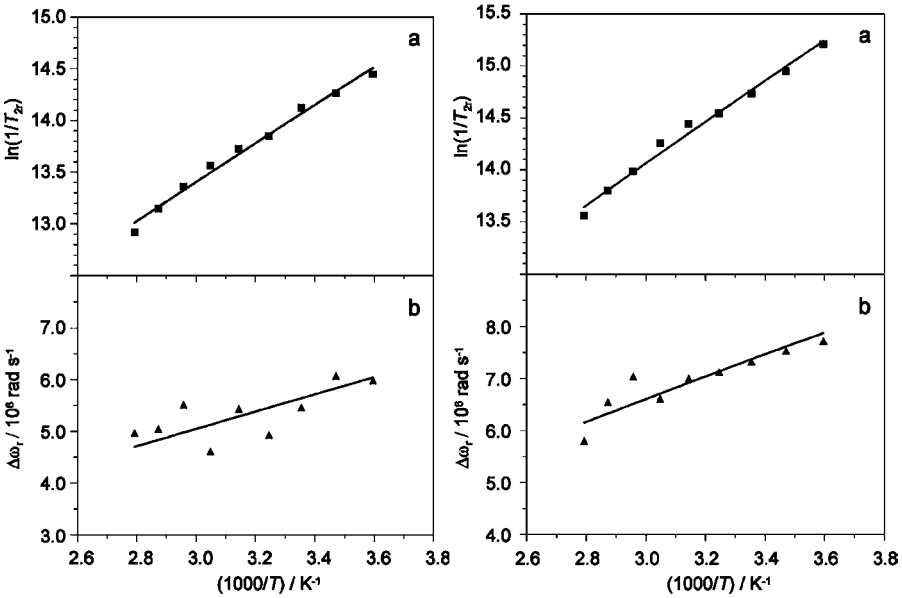

Figure 11. Variable-temperature ^{17}O transverse relaxation rates (a) and chemical shifts (b) obtained for $[Mn(\mathbf{L}^1)(H_2O)]^+$ (left) and $[Mn(\mathbf{L}^2)(H_2O)]$ (right). c_{MnL} = 5 mM, 0.1 M TRIS, pH 8.0. The full lines represent the best simultaneous fit of the ^{17}O NMR and ^1H NMRD data.

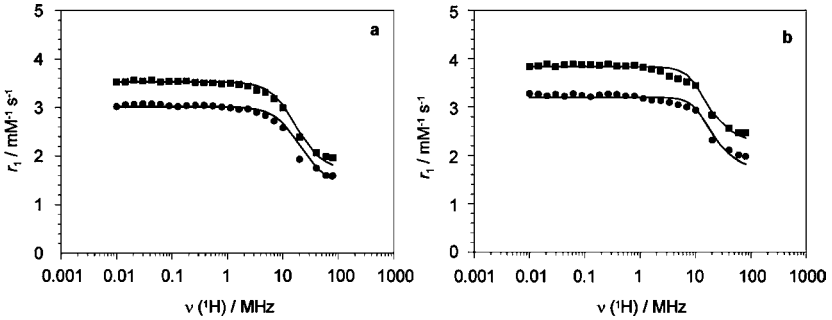

Figure 12. ^1H NMRD profiles of $[Mn(\mathbf{L}^1)(H_2O)]^+$ (a) and $[Mn(\mathbf{L}^2)(H_2O)]$ (b) measured at 25 (■) and 37 °C (●) (c_{MnL} = 5 mM, 0.1 M TRIS, pH 8.0).

Table 7. Relaxivity and Best-Fit Parameters Obtained from the Simultaneous Analysis of ^{17}O NMR and ^1H NMRD Data for MnL^1 and MnL^2 Compared with Those for Other Relevant Mn^{2+} Chelates and the Hexaaqua Mn^{2+} Ion

parameter	$[Mn(\mathbf{L}^1)(H_2O)]^+$	$[Mn(\mathbf{L}^2)(H_2O)]$	[Mn(**15-py N_3O_2**)$(H_2O)_2]^{2+}$ [b]	$[Mn(\mathbf{15\text{-}py\ N_5})(H_2O)_2]^{2+}$ [b]	[Mn(**9-ane N_2O-2A**)$(H_2O)_x$] [c]	[Mn(**9-ane N_2O-2P**)$(H_2O)]^{2-}$ [c]	$[Mn_2(enota)(H_2O)_2]$ [d]	$[Mn(H_2O)_6]^{2+}$ [e]
CN	6	6	7	7	6/7	6	6	6
r_1/mM^{-1} s^{-1} [a]	2.39/1.94	2.84/2.32	4.48/3.61	3.56/3.13	2.83/2.30	5.08/4.29	3.39/2.71	7.4[d]/6.76[e]
k_{ex}^{298}/10^7 s^{-1}	303 ± 19	177 ± 9	0.38	6.9	119	1.20	5.5	2.1
$\Delta H^{\ddagger}$/kJ mol^{-1}	13.0 ± 1.6	14.0 ± 1.2	35.3	37.7	11.7	38.8	20.5	32.9
$\Delta S^{\ddagger}$/J mol^{-1} K^{-1}	−20 ± 3	−21 ± 2	−1.0	+32	−31.7	20.5	−28	+5.7
$\Delta V^{\ddagger}$/cm^3 mol^{-1} [g]	−5.4 ± 0.3	−4.9 ± 0.2	−0.1 ± 0.1[h]	+1.6 ± 0.1[h], +3.2[f]	+5.1 ± 0.2[h]	−4.4 ± 0.1[h]	−10.7	−5.7
E_{rH}/kJ mol^{-1}	16.0 ± 2.6	20.3 ± 2.1	16.1	23.1	12	23	18	
τ_{rH}^{298}/ps	23.0 ± 1.8	38.6 ± 1.9	40.3	28.3	22	99	26	30[f]
τ_v^{298}/ps	8.7 ± 0.8	14.3 ± 0.6	3.3	3.9	12.4	30.7	7.7	3.3
Δ^2/10^{18} s^{-2}	40.0 ± 5	302 ± 11	6.6	4.6	79	60	4.7	5.6
$A_O/\hbar$/10^6 rad s^{-1}	36.6 ± 1.3	39.9 ± 1.7	38.6	38.6	33.3	33.3	32.7	33.3

[a] 20 MHz and 25/37 °C. [b] Ref 27. [c] Ref 28. [d] Ref 22 . [e] Ref 59. [f] Ref 60. [g] The real errors for $\Delta V^{\ddagger}$ are higher than those obtained from the fitting (in the table) and estimated values are about ±1 cm^3 mol^{-1}. [h] This work.

water exchange rates were typically found about 2 orders of magnitude lower (k_{ex} ~10^7 s^{-1}) for Mn^{2+} complexes as shown in Table 7. In comparison to $[Mn(H_2O)_6]^{2+}$, the water exchange is usually accelerated upon complexation. In general, the rate of water exchange is related to the donor/acceptor abilities of the ligands and to the charge distribution in the molecule. Ligands HL^1 and H_2L^2 have a strong donor ability resulting in a strong ligand field (tendency to oxidize to Mn^{3+}). Water binding is predominantly based on Coulombic interaction which is weakened by the repulsion of the neighboring negative charge represented by the functional group (carboxylate/phosphonate).

dx.doi.org/10.1021/ic201935r | Inorg. Chem. 2011, 50, 12785–12801

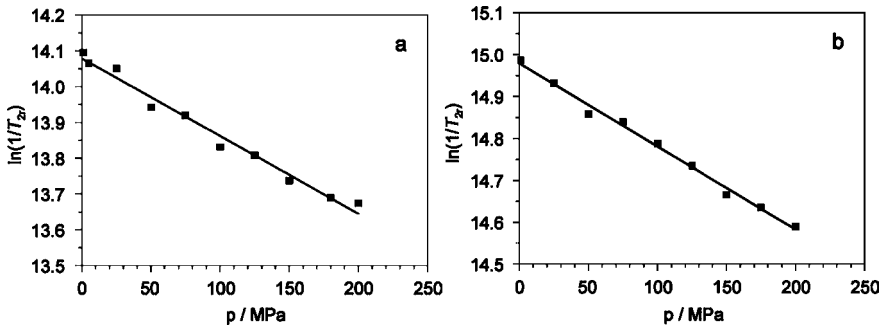

Figure 13. Variable-pressure reduced ^{17}O transverse relaxation rates measured for Mn**L**^{1} (a) and Mn**L**^{2} (b) at 295 K and 9.4 T. The full line represents the result of the data fit as described in the text.

The mechanism of the water exchange was determined by variable-pressure ^{17}O transverse relaxation rate measurements. Under constant temperature and magnetic field, the variation of $1/T_2$ with pressure is related to the acceleration or deceleration of the water exchange process. The pressure dependence of k_{ex} is defined in eq 5 where $\Delta V^{\ddagger}$ is the activation volume for the water exchange and $(k_{ex})_0^T$ is the water exchange rate at zero pressure and temperature T.

$$\frac{1}{\tau_m} = k_{ex} = (k_{ex})_0^T \exp\left\{-\frac{\Delta V^{\ddagger}}{RT}P\right\} \quad (5)$$

The activation volume is the most significant parameter to directly assess the mechanism.[62] A positive value of the activation volume indicates an associative (A) or associative interchange (I_a) mechanism, whereas a negative value accounts for a dissociative (D) or dissociative interchange mechanism (I_d). Variable-pressure transverse ^{17}O relaxation rate data were collected for Mn**L**^{1} and Mn**L**^{2} (displayed in Figure 13) as well as for complexes of other ligands that we have previously reported (15- and 9-membered macrocycles, see Supporting Information, Figure S1). The data were fitted to eq 5 and to the equations describing $1/T_{2r}$ relaxation (see Supporting Information). We assumed that $A_O/\hbar$ and τ_v are pressure-independent. The contribution of the electronic relaxation to $1/T_{2r}$ is so small that an eventual pressure dependence of τ_{v0} would not influence the activation volume of the water exchange. For $\Delta V^{\ddagger}$, an error of ± 1 cm^3 mol^{-1} or 10% is usually considered to be realistic. The activation volumes calculated for Mn**L**^{1}, Mn**L**^{2}, and for the previously studied complexes are listed in Table 7 (calculated $(k_{ex})_0^T$ values are given in the Supporting Information, Table S3). The negative activation volumes for Mn**L**^{1}, Mn**L**^{2}, and Mn(9-aneN$_2$O-2P) evidence an associatively activated mechanism for the water exchange. This is in full accordance with previously reported data for complexes with a coordination number of 6 where an associative mechanism has been proven (ENOTA, hexaaqua ion). The associative activation mode implies an increase of the coordination number to 7 (which is also common for Mn^{2+}) in the transition state, which is more probable than a dissociative mechanism involving penta-coordinated Mn^{2+} species. On the other hand, the small positive activation volume for Mn(15-pyN$_5$) (CN = 7) evidence a dissociative interchange mechanism for the water exchange. Analogously, a dissociative mechanism was found for previously studied seven-coordinate complexes like $[Mn(edta)]^{2-}$ ($\Delta V^{\ddagger} = 3.4$ cm^3 mol^{-1}),[63] where the transition state involves a coordination number of 6 for Mn^{2+}. Mn(9-aneN$_2$O-2A) is present in an equilibrium between mono- and bishydrated species, where the bishydrated species are in majority. The water exchange rate, reported previously,[28] and the activation volume, measured here, are average values of the contributions originating from the mono- and bishydrated species. We should note that the pressure also certainly influences the hydration equilibrium (shifted to the bishydrated species with increasing pressure). Therefore the exact interpretation of the activation volume is difficult, though it shows that a dissociatively activated mechanism prevails. The close-to-zero activation volume for Mn(15-pyN$_3$O$_2$) indicates an almost pure concerted mechanism (I). In general, the measured activation volumes of the complexes studied are small (far from the limiting values, $\Delta V^{\ddagger} = \pm 13$ cm^3 mol^{-1})[62] and thus correspond to associative interchange (I_a) or dissociative interchange (I_d) mechanisms. This is particularly valid for the complexes of the 15-membered ligands that possess a more "open" structure and also a weak interaction between the coordinated water molecules and the oxygen donor atoms in 15-pyN$_3$O$_2$).[27] The mechanism as assessed from the activation volumes for Mn**L**^{1}, Mn**L**^{2}, Mn(15-pyN$_3$O$_2$), and Mn(15-pyN$_5$) are also supported by the activation entropies.

The ^{17}O chemical shifts are proportional to the hydration number and to the hyperfine coupling constant, $A_O/\hbar$, which reflects the manganese spin density on the oxygen nucleus. Its value is expected to remain in a limited range for common Mn^{2+} complexes. The values of $A_O/\hbar$ obtained from the fit, 36.6 and 39.9 $\times$ 10^6 rad s^{-1} for Mn**L**^{1} and Mn**L**^{2}, respectively, agree with those for other Mn^{2+} complexes (33−40 $\times$ 10^6 rad s^{-1}) which justifies the hydration number $q = 1$ for both complexes. We should note, however, that for Mn**L**^{2} an outer-sphere contribution had to be included to the ^{17}O chemical shifts to account for the elevated chemical shifts (described by an empirical constant, $C_{os} = 0.2$). The higher chemical shifts can be also a consequence of a small second sphere effect, which is induced by the presence of the phosphonate group. Since the description of such a second sphere effect is rather difficult, and it represents a limited contribution, we prefer to include it as an outer sphere contribution to the chemical shift.

The shape of the ^1H NMRD profiles corresponds to typical low-molecular-weight chelates with one dispersion between 1−10 MHz. The relaxivities over the whole magnetic field range are slightly lower than what is usually observed for monohydrated Mn^{2+} chelates. This difference can be related to the very high value of Δ^2 (trace of the squares of the transient ZFS tensor), likely caused by the higher electronic density on the nitrogen atoms (higher ligand field) induced by the electron donating pendant arms and the pyridine core.

dx.doi.org/10.1021/ic201935r | Inorg. Chem. 2011, 50, 12785−12801

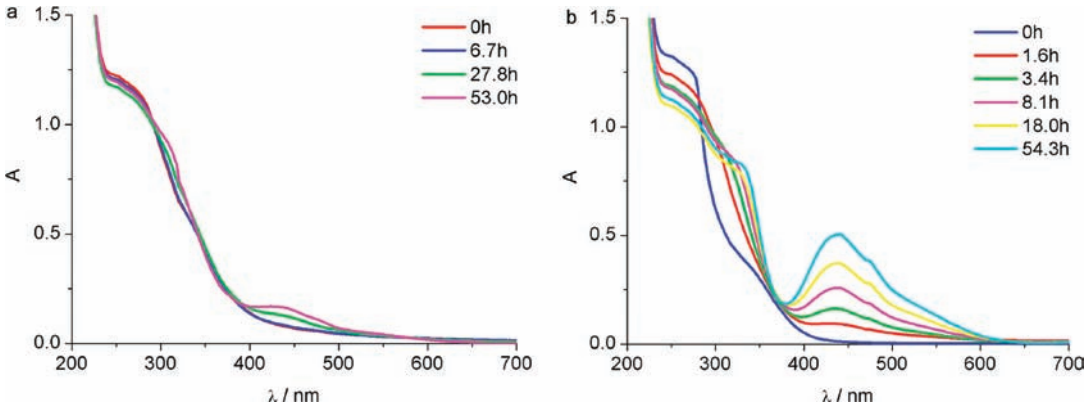

Figure 14. UV−vis spectra of the solutions ($c_{Mn2+} = c_L$ = 5 mM, pH = 8.0, 0.1 M TRIS) of Mn^{2+} complexes with HL^1 (a) and H_2L^2 (b) open to air atmosphere recorded over time.

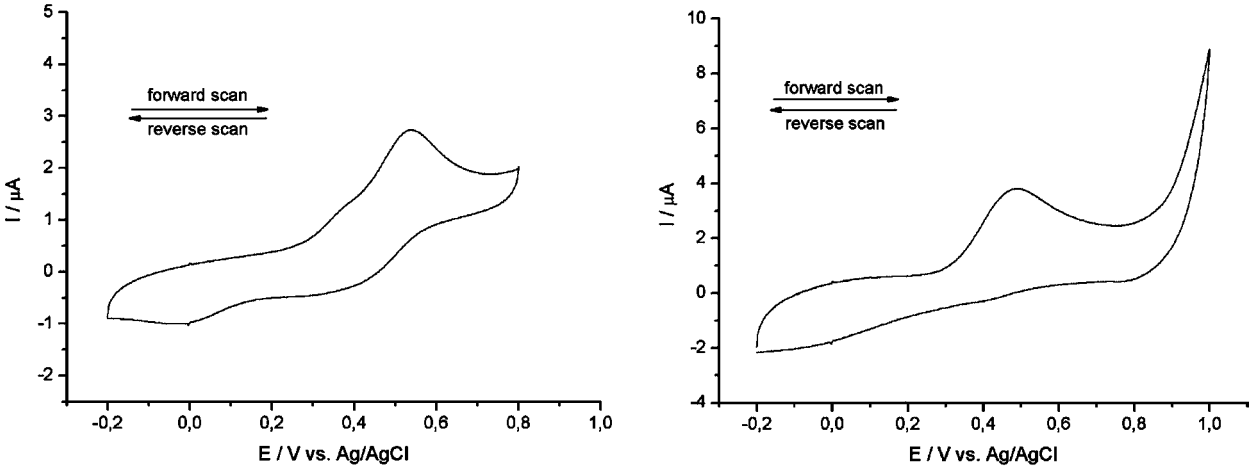

Figure 15. Cyclic voltammograms of MnL^1(a) and MnL^2(b) (0.05 M KCl, pH = 8.0, 100 mV s^{-1}).

The relaxivities at 20 MHz (Table 7) also reflect the difference in the hydration state: MnL^1 and MnL^2 with one coordinated water molecule have about 50% lower relaxivity than the bishydrated complexes of 15-membered macrocycles. The phosphonate moiety has a positive effect on the relaxivity which is higher for MnL^2 than for MnL^1 (higher τ_r and possible second-sphere effect). However, the relaxivities of both complexes are lower than those of the commercially used monohydrated $[Gd(dota)(H_2O)]^-$ and $[Gd(dtpa)(H_2O)]^{2-}$.

Anion Binding Study. It is known that in bishydrated complexes, small bidentate endogenous anions like phosphate, carbonate, or citrate are capable of replacing the two inner-sphere water molecules if they are coordinated in adjacent position, such as in $[Gd(do3a)(H_2O)_2]$, which can be detrimental for in vivo relaxivity. For the monohydrated Mn^{2+} complexes of HL^1 and H_2L^2, anion binding should not be significant. This was proved by proton relaxivity measurements in the presence of 1−50 equiv of phosphate (mixture of $HPO_4^{2-}/H_2PO_4^-$ at pH 8.0), carbonate (CO_3^{2-}/HCO_3^-), or citrate ($cit^{3-}/Hcit^{2-}$) (see Supporting Information, Figure S2). The invariance of the relaxivities proves that they are sufficiently inert toward substitution of the inner-sphere water molecule by small endogenous anions.

Oxidation State Mn^{3+}. The solutions of MnL^1 and, in particular, of MnL^2 complexes undergo a color change after several hours upon manipulation in air. The UV−vis spectra recorded over time (Figure 14) revealed the increase of the absorbance at 440 nm for both complexes which we related to the oxidation of Mn^{2+} to Mn^{3+} by air oxygen. This oxidation resulting in low-spin Mn^{3+} can dramatically reduce the relaxivity of the complex as was indeed proven by recording the ^1H NMRD profile before and after exposure to air (see Supporting Information, Figure S3). To confirm the oxidation, we investigated both systems by cyclic voltammetry. The voltammograms recorded for MnL^1 and MnL^2 (Figure 15) exhibit only the oxidation peaks at potentials E_{ox} = 0.73 V for MnL^1 and E_{ox} = 0.68 V for MnL^2 (vs SHE) illustrating irreversible processes. The oxidation peak potential is higher for MnL^1 than for MnL^2 which indicates that the divalent oxidation state is more stable with HL^1 than with H_2L^2. Because of the *+I* effect, the deprotonated phosphonate renders $(L^2)^{2-}$ anion more electron rich and provides a stronger ligand field in comparison to $(L^1)^{1-}$ anion. This can consequently lead to a stronger stabilization of the oxidation state +III (Mn^{3+} complex), thus to a higher tendency of oxidation of complex with H_2L^2 than with HL^1. This observation is in good agreement with the time-dependent UV−vis spectra showing indeed faster oxidation of MnL^2 by air oxygen.

The absence of the reduction peaks could be explained by a very fast diffusion of the oxidized form of the complex away from the proximity of electrode; however, a higher scan rate of 200 mV s^{-1} (faster electron transfer) gave identical results. In contrast to the monohydrated nature of the Mn^{2+} complexes, at the experimental pH 8, the Mn^{3+} complex likely exists as a

dx.doi.org/10.1021/ic201935r | *Inorg. Chem.* 2011, 50, 12785−12801

mono(hydroxo) complex, also supported by the X-ray structure of $[Mn(\mathbf{L}^2)(OH)]$ (see Figure 5). The deprotonation of the active species can then lead to a slow kinetics of the reverse half-reaction or some binding on the electrode surface which can be responsible of the irreversibility.

Since data on Mn^{3+} aminoacetate complexes are scarce, here we compare the results with those for Mn^{2+} complexes of NOTA (E = 0.74 V, ΔE = 94 mV) or NOTPr (E = 0.49 V, ΔE = 68 mV).[64] MnNOTA is air-stable, while the propionate analogue readily forms a red solution containing the Mn^{3+} complex. The oxidation peak potentials for MnNOTA E_{ox} = 0.79 V and MnNOTPr E_{ox} = 0.52 V flank the E_{ox} for $Mn\mathbf{L}^1$ and $Mn\mathbf{L}^2$. Thus, all characterization techniques employed here confirm that both complexes are oxidized by air-oxygen, $Mn\mathbf{L}^2$ several times faster than $Mn\mathbf{L}^1$. Therefore, all NMR measurements were carried out with deoxygenated solutions prepared under argon atmosphere (or small amount of hydroxylamine as reducing agent was added).

CONCLUSIONS

12-membered cycles containing a pyridine ring and an acetic ($H\mathbf{L}^1$) or a methylphosphonic acid ($H_2\mathbf{L}^2$) pendant arm were synthesized, and the Mn^{2+} complexes were characterized with respect to potential application as MRI contrast enhancing agents. The synthetic approach using nosyl or tosyl amino-protecting groups (starting compounds diethylenetriamine or tosylaziridine, respectively) gave good yields. The crystal structures of $Mn\mathbf{L}^1$ and $Mn\mathbf{L}^2$ confirmed CN = 6 for Mn^{2+}. The basicity of the ligand is reduced by the presence of the pyridine ring. The functional group in the pendant arm significantly increases ligand basicity; this effect is more important for the phosphonate than for the acetate. ^1H and ^{31}P pH-NMR titrations revealed that the first two protonation steps (log K_{H1} and log K_{H2}) of $H\mathbf{L}^1$ and $H_2\mathbf{L}^2$ occur on the macrocyclic amino groups (accompanied by a proton transfer from the tertiary to a secondary amino group during the second protonation step) followed by protonation of the functional group. $Mn\mathbf{L}^2$ shows about 2 orders of magnitude higher stability than $Mn\mathbf{L}^1$ reflecting the increased basicity of $H_2\mathbf{L}^2$. In comparison with the previous data, the extension of the macrocyclic cavity from a 9- to a 12- or 15-membered ring and the presence of the pyridine (rigidity) also increases the stability of the Mn^{2+} complexes. Thus, $Mn\mathbf{L}^1$ and $Mn\mathbf{L}^2$ show good thermodynamic stability, comparable to that of MnEDTA. Nevertheless, they remain less stable than complexes of hexa-, hepta-, or octadentate ligands such as NOTA, PCTA, or DOTA. The dissociation of $Mn\mathbf{L}^1$ is very fast (k_{obs} = 1−12 × 10^3 s^{-1}) in comparison to previously measured Mn^{2+} or Gd^{3+} complexes, and proceeds exclusively via the spontaneous and proton-assisted dissociations of the mono-protonated complex. Zn^{2+} has no influence on the overall dissociation rate. Despite its higher thermodynamic stability, $Mn\mathbf{L}^2$ is kinetically more labile and dissociates instantaneously (pH 5.1−6.2, Zn^{2+} excess).

Aqueous solutions of $Mn\mathbf{L}^1$ and $Mn\mathbf{L}^2$ are prone to oxidation under air atmosphere. The formation of Mn^{3+} species was monitored by UV−vis spectra and confirmed by ^1H NMRD and by the crystal structure of $[Mn(\mathbf{L}^2)(OH)]\cdot 0.5LiCl\cdot 7H_2O$. Cyclic voltammetry evidenced low oxidation peak potentials for both complexes at the limit of possible air-oxidation.

The variable-temperature ^{17}O NMR and ^1H NMRD data resulted in the parameters governing proton relaxivity. Very fast water exchange, k_{ex} = 3.03 and 1.77 × 10^9 s^{-1}, was found for $Mn\mathbf{L}^1$ and $Mn\mathbf{L}^2$, respectively. The negative activation volumes, $\Delta V^{\ddagger}$, obtained from variable-pressure ^{17}O NMR measurements indicate an associatively activated water exchange. The ^{17}O chemical shifts confirmed a hydration number of one for both complexes.

In overall, the higher basicity of the 12-membered ligands studied here provides higher thermodynamic stability for the Mn^{2+} complexes with respect to the 9- or 15-membered analogues, but also leads to an increased tendency of oxidation to Mn^{3+} species. On the basis of these results and our previous data, we can draw some general conclusions. Within the family of polyazamacrocyclic ligands, by varying the macrocycle size and the nature of the donor atoms in the macrocycle or in the pendant arm, one can significantly modify the thermodynamic, redox, and kinetic stability as well as the hydration number of the Mn^{2+} complexes. Unfortunately, these factors could not be all simultaneously optimized; the improvement of one parameter is accompanied by a detrimental effect on another. To develop highly stable and efficient Mn^{2+}-based contrast agents, further research should likely focus on more rigid complexes.

ASSOCIATED CONTENT

Supporting Information

The overall protonation/stability constants (log β_{hlm}) of both ligands and their complexes, values of first-order-rate constants for dissociation of $Mn\mathbf{L}^2$, calculated values of the activation volumes and the water exchange rate at zero pressure, variable-pressure ^{17}O NMR data for previously studied ligands, ^1H relaxivities upon addition of phosphate, carbonate, or citrate to solutions of $Mn\mathbf{L}^1$ and $Mn\mathbf{L}^2$, ^1H NMRD profiles of $Mn\mathbf{L}^2$ recorded before and after exposure to air, and equations used for treatment of the relaxometric data. This material is available free of charge via the Internet at http://pubs.acs.org.

AUTHOR INFORMATION

Corresponding Author

*Fax: +33 2 38 63 15 17 (E.T.), +420 2 2195 1253 (I.L.). Phone: +33 2 38 25 76 25 (E.T.), +420 2 2195 1259 (I.L.). E-mail: eva.jakabtoth@cnrs-orleans.fr (E.T.), lukes@natur.cuni.cz (I.L.).

ACKNOWLEDGMENTS

The Long-Term Research Plan of the Ministry of Education of the Czech Republic (No. MSM0021620857), the Ligue National Contre le Cancer and the Agence Nationale de la Recherche (France) are acknowledged for financial support. B. Drahoš acknowledges the PhD grant of the RFR program of the French Ministry of Education and Research. The work was carried out in the frame of COST D38 (MŠMT OC 179), COST CM0802 (PhoSciNet) and the Grant Agency of the Czech Republic (No. P207/11/1437). We thank to J. Havlíčková and V. Kubíček for helping with potentiometric titrations, Prof. J. Barek and Dr. V. Vyskočil for providing electrochemical equipment.

REFERENCES

(1) Schwert, D. D.; Davies, J. A.; Richardson, N. Non-gadolinium based MRI contrast agents. In *Contrast agents I: magnetic resonance imaging*; Krause, W., Ed.; Springer: Berlin, Germany, 2002; pp 165−200.

(2) Kubíček, V.; Tóth, É. *Adv. Inorg. Chem.* **2009**, *61*, 63−129.

(3) Caravan, P.; Ellison, J. J.; McMurry, T. J.; Lauffer, R. B. *Chem. Rev.* **1999**, *99*, 2293−2352.
(4) Tóth, É., Merbach, A. E. *The Chemistry of Contrast Agents in Medical Magnetic Resonance Imaging*; John Wiley & Sons: Chichester, U.K., 2001.
(5) Hermann, P.; Kotek, J.; Kubíček, V.; Lukeš, I. *Dalton Trans.* **2008**, 3027−3047.
(6) Sherry, A. D.; Caravan, P.; Lenkinski, R. E. *J. Magn. Reson. Imag.* **2009**, *30*, 1240−1248.
(7) Bannister, J. V.; Bannister, W. H.; Rotilio, G. *Crit. Rev. Biochem.* **1976**, *22*, 111−180.
(8) Wedler, F. C.; Denman, R. B. *Curr. Top. Cell Regul.* **1984**, *24*, 153−169.
(9) Aschner, M.; Erikson, K. M.; Dorman, D. C. *Crit. Rev. Toxicol.* **2005**, *35*, 1−32.
(10) *NMR Biomed.* **2004**, *17*, 527−634. The issue No. 8 is dedicated to the Manganese Enhanced Magnetic Resonance Imaging (MEMRI).
(11) Bock, N. A.; Silva, A. C. *Future Neurol.* **2007**, *2*, 297−305.
(12) Cersosimo, M. G.; Koller, W. C. *NeuroToxicology* **2006**, *27*, 340−346.
(13) Gallez, B.; Baudelet, C.; Geurts, M. *Magn. Reson. Imag.* **1998**, *16*, 1211−1215.
(14) Drahoš, B.; Kubíček, V.; Bonnet, C. S.; Hermann, P.; Lukeš, I.; Tóth, É. *Dalton Trans.* **2011**, *40*, 1945−1951.
(15) Rocklage, S. M.; Cacheris, W. P.; Quay, S. C.; Hahn, F. E.; Raymond, K. N. *Inorg. Chem.* **1989**, *28*, 477−485.
(16) Koenig, S. H.; Baglin, C.; Brown, R. D.; Brewer, C. F. *Magn. Reson. Med.* **1984**, *1*, 496−501.
(17) Troughton, J. S.; Greenfield, M. T.; Greenwood, J. M.; Dumas, S.; Wiethoff, A. J.; Wang, J.; Spiller, M.; McMurry, T. J.; Caravan, P. *Inorg. Chem.* **2004**, *43*, 6313−6323.
(18) Aime, S.; Anelli, P. L.; Botta, M.; Brocchetta, M.; Canton, S.; Fedeli, F.; Gianolio, E.; Terreno, E. *J. Biol. Inorg. Chem.* **2002**, *7*, 58−67.
(19) Maigut, J.; Meier, R.; Zahl, A.; van Eldik, R. *Inorg. Chem.* **2008**, *47*, 5702−5719.
(20) Bertin, A.; Steibel, J.; Michou-Gallani, A.-I.; Gallani, J.-L.; Felder-Flesch, D. *Bioconjugate Chem.* **2009**, *20*, 760−767.
(21) Geraldes, C. F. G. C.; Sherry, A. D.; Brown, R. D.; Koenig, S. H. *Magn. Reson. Med.* **1986**, *3*, 242−250.
(22) Balogh, E.; He, Z.; Hsieh, W.; Liu, S.; Tóth, É. *Inorg. Chem.* **2007**, *46*, 238−250.
(23) Bianchi, A.; Calabi, L.; Giorgi, C.; Losi, P.; Mariani, P.; Palano, D.; Paoli, P.; Rossi, P.; Valtancoli, B. *J. Chem. Soc., Dalton Trans.* **2001**, 917−922.
(24) Wang, S.; Westmoreland, T. D. *Inorg. Chem.* **2009**, *48*, 719−728.
(25) Tei, L.; Gugliotta, G.; Fekete, M.; Kálmán, F. K.; Botta, M. *Dalton Trans.* **2011**, *40*, 2025−2032.
(26) (a) Newton, J. E.; Jackels, F. C. *J. Coord. Chem.* **1988**, *19*, 265−277. (b) Jackels, S. C.; Durham, M. M.; Newton, J. E.; Henninger, T. C. *Inorg. Chem.* **1992**, *31*, 234−239.
(27) Drahoš, B.; Kotek, J.; Hermann, P.; Lukeš, I.; Tóth, É. *Inorg. Chem.* **2010**, *49*, 3224−3238.
(28) Drahoš, B.; Pniok, M.; Kotek, J.; Hermann, P.; Lukeš, I.; Tóth, E. *Dalton Trans.* **2011**, *40*, 10131−10146.
(29) Perrin, D. D. *Purification of Laboratory Chemicals*; Pergamon Press: Oxford, U.K., 1988.
(30) Gali, H.; Prabhu, K. R.; Karra, S. R.; Katti, K. V. *J. Org. Chem.* **2000**, *65*, 676−680.
(31) Bieber, L. W.; de Araújo, M. C. F. *Molecules* **2002**, *7*, 902−906.
(32) Aime, S.; Botta, M.; Frullano, L.; Geninatti Crich, S.; Giovenzana, G.; Pagliarin, R.; Palmisano, G.; Sirtori, F. R.; Sisti, M. *J. Med. Chem.* **2000**, *43*, 4017−4024.
(33) Siaugue, J. M.; Segat-Dioury, F.; Sylvestre, I.; Favre-Réguillon, A.; Foos, J.; Madic, C.; Guy, A. *Tetrahedron* **2001**, *57*, 4713−4718.
(34) Baker, W.; Buggle, K. M.; McOmie, J. F. W.; Watkins, D. A. M. *J. Chem. Soc.* **1958**, 3594−3603.
(35) Dioury, F.; Ferroud, C.; Guya, A.; Port, M. *Tetrahedron* **2009**, *65*, 7573−7579.
(36) (a) Otwinovski, Z.; Minor, W. *HKL Denzo and Scalepack Program Package*; Nonius BV: Delft, The Netherlands, 1997; (b) Otwinovski, Z.; Minor, W. *Methods Enzymol.* **1997**, *276*, 307−326.
(37) Altomare, A.; Cascarano, G.; Giacovazzo, C.; Guagliardi, A.; Burla, M. C.; Polidori, G.; Camalli, M. *J. Appl. Crystallogr.* **1994**, *27*, 435−435.
(38) Sheldrick, G. M. *SHELXL97, A Computer Program for Refinement of Crystal Structures*; University of Göttingen, Göttingen, Germany, 1997.
(39) Kývala, M.; Lukeš, I. *Proceedings of the International Conference on Chemometrics '95*, Pardubice, Czech Republic, 1995; p 63.
(40) Kývala, M.; Lubal, P.; Lukeš, I. *IX. Spanish−Italian and Mediterranean Congress on Thermodynamics of Metal Complexes (SIMEC 98)*, Girona, Spain, 1998. The full version of the OPIUM program is available (free of charge) on http://web.natur.cuni.cz/~kyvala/opium.html.
(41) (a) Martell, A. E.; Smith, R. M. *Critical Stability Constants*; Plenum Press: New York, 1974−1989; Vols. *1*−*6*. (b) NIST Standard Reference Database 46 (*Critically Selected Stability Constants of Metal Complexes*), Version 7.0, 2003. (c) Baes, C. F., Jr.; Mesmer, R. E. *The Hydrolysis of Cations*; Wiley: New York, 1976.
(42) (a) Táborský, P.; Lubal, P.; Havel, J.; Kotek, J.; Rudovský, J.; Hermann, P.; Lukeš, I. *Collect. Czech. Chem. Commun.* **2005**, *70*, 1909−1942. (b) Försterová, M.; Svobodová, I.; Lubal, P.; Táborský, P.; Kotek, J.; Hermann, P.; Lukeš, I. *Dalton Trans.* **2007**, 535−549.
(43) Raiford, D. S.; Fisk, C. L.; Becker, E. D. *Anal. Chem.* **1979**, *51*, 2050−2051.
(44) Vold, R. L.; Waugh, J. S.; Klein, M. P.; Phelps, D. E. *J. Chem. Phys.* **1968**, *48*, 3831−3832.
(45) Meiboom, S.; Gill, D. *Rev. Sci. Instrum.* **1958**, *29*, 688−691.
(46) Hugi, A. D.; Helm, L.; Merbach, A. E. *Helv. Chim. Acta* **1985**, *68*, 508−521.
(47) Cusanelli, A.; Nicula-Dadci, L.; Frey, U.; Merbach, A. E. *Inorg. Chem.* **1997**, *36*, 2211−2217.
(48) Ducommun, Y.; Earl, W. L.; Merbach, A. E. *Inorg. Chem.* **1979**, *18*, 2754−2759.
(49) Siaugue, J. M.; Segat-Dioury, F.; Sylvestre, I.; Favre-Réguillon, A.; Foos, J.; Madic, C.; Guy, A. *Tetrahedron* **2001**, *57*, 4713−4718.
(50) Lukeš, I.; Kotek, J.; Vojtíšek, P.; Hermann, P. *Coord. Chem. Rev.* **2001**, *216*−*217*, 287−312.
(51) Costa, J.; Delgado, R. *Inorg. Chem.* **1993**, *32*, 5257−5265.
(52) Kim, W. D.; Hrncir, D. C.; Kiefer, G. E.; Sherry, A. D. *Inorg. Chem.* **1995**, *34*, 2225−2232.
(53) Delgado, R.; Quintino, S.; Teixeira, M.; Zhang, A. *J. Chem. Soc., Dalton Trans.* **1997**, 55−63.
(54) Geraldes, C. F. G. C.; Sherry, A. D.; Cacheris, W. P. *Inorg. Chem.* **1989**, *28*, 3336−3341.
(55) Geraldes, C. F. G. C.; Sherry, A. D.; Marques, M. P. M.; Alpoim, M. C.; Cortes, S. *J. Chem. Soc., Perkin Trans. 2* **1991**, 137−146.
(56) Rohovec, J.; Kývala, M.; Vojtíšek, P.; Hermann, P.; Lukeš, I. *Eur. J. Inorg. Chem.* **2000**, 195−203.
(57) Huskens, J.; Sherry, A. D. *J. Am. Chem. Soc.* **1996**, *118*, 4396−4404.
(58) Sarka, L.; Burai, L.; Brücher, E. *Chem.—Eur. J.* **2000**, *6*, 719−724.
(59) Ducommun, Y.; Newmann, K. E.; Merbach, A. E. *Inorg. Chem.* **1980**, *19*, 3696−3703.
(60) Dees, A.; Zahl, A.; Puchta, R.; van Eikema Hommes, N. J. R.; Heinemann, F. W.; Ivanović-Burmazović, I. *Inorg. Chem.* **2007**, *46*, 2459−2470.
(61) Zetter, M. S.; Grant, M.; Wood, E. J.; Dodgen, H. W.; Hunt, J. P. *Inorg. Chem.* **1972**, *11*, 2701−2706.
(62) Helm, L.; Merbach, A. E. *Chem. Rev.* **2005**, *105*, 1923−1959.
(63) Maigut, J.; Meier, R.; Zahl, A.; van Eldik, R. *J. Am. Chem. Soc.* **2008**, *130*, 14556−14569.
(64) Fukuda, Y.; Hirota, M.; Kon-no, M.; Nakao, A.; Umezawa, K. *Inorg. Chim. Acta* **2002**, *339*, 322−326.